



Deposited via The University of Sheffield.

White Rose Research Online URL for this paper:

<https://eprints.whiterose.ac.uk/id/eprint/117038/>

Version: Accepted Version

Article:

Erickson, T., Morgan, C.P, Olt, J. et al. (2017) Integration of Tmc1/2 into the mechanotransduction complex in zebrafish hair cells is regulated by Transmembrane O-methyltransferase (Tomt). *Elife*, 6.

<https://doi.org/10.7554/eLife.28474>

Reuse

Items deposited in White Rose Research Online are protected by copyright, with all rights reserved unless indicated otherwise. They may be downloaded and/or printed for private study, or other acts as permitted by national copyright laws. The publisher or other rights holders may allow further reproduction and re-use of the full text version. This is indicated by the licence information on the White Rose Research Online record for the item.

Takedown

If you consider content in White Rose Research Online to be in breach of UK law, please notify us by emailing eprints@whiterose.ac.uk including the URL of the record and the reason for the withdrawal request.

1 **Title**

2 Integration of Tmc1/2 into the mechanotransduction complex in zebrafish hair cells is regulated by
3 Transmembrane O-methyltransferase (Tomt)

4

5 **Running title**

6 Tomt is required for mechanotransduction

7

8 **Authors**

9 Timothy Erickson¹, Clive P. Morgan¹, Jennifer Olt², Katherine Hardy², Elisabeth Busch-Nentwich³,
10 Reo Maeda¹, Rachel Clemens¹, Jocelyn F. Krey¹, Alex Nechiporuk⁴, Peter G. Barr-Gillespie¹, Walter
11 Marcotti², Teresa Nicolson¹

12

13 1) Oregon Hearing Research Center and the Vollum Institute, Oregon Health & Science University,
14 Portland, OR; 2) Department of Biomedical Science, University of Sheffield, Sheffield, UK; 3)
15 Wellcome Trust Sanger Institute, Cambridge, UK; 4) Department of Cell, Developmental & Cancer
16 Biology, Oregon Health & Science University, Portland, OR.

17

18

19 **Abstract**

20 Transmembrane O-methyltransferase (*TOMT / LRTOMT*) is responsible for non-syndromic deafness
21 DFNB63. However, the specific defects that lead to hearing loss have not been described. Using a
22 zebrafish model of DFNB63, we show that the auditory and vestibular phenotypes are due to a lack
23 of mechanotransduction (MET) in *Tomt*-deficient hair cells. GFP-tagged *Tomt* is enriched in the Golgi
24 of hair cells, suggesting that *Tomt* might regulate the trafficking of other MET components to the
25 hair bundle. We found that *Tmc1/2* proteins are specifically excluded from the hair bundle in *tomt*
26 mutants, whereas other MET complex proteins can still localize to the bundle. Furthermore, mouse
27 TOMT and TMC1 can directly interact in HEK 293 cells, and this interaction is modulated by His183 in
28 TOMT. Thus, we propose a model of MET complex assembly where *Tomt* and the *Tmcs* interact
29 within the secretory pathway to traffic *Tmc* proteins to the hair bundle.

30

31

32 **Introduction**

33

34 Mechanoelectrical transduction (MET) is the process by which sensory hair cells convert mechanical
35 force such as auditory and vestibular stimuli into electrical signals. The mechanosensitive organelle
36 of the hair cell is the hair bundle, an apical collection of actin-filled stereocilia arranged in a staircase
37 fashion. These stereocilia are tethered by intercilial links, including a *trans* heteromeric complex of
38 Cadherin 23 (CDH23) - Protocadherin 15 (PCDH15) called the tip link (Kazmierczak et al., 2007). One
39 potential location of the MET channel complex is at the lower end of the tip link where PCDH15
40 resides (Beurg et al., 2009). A commonly accepted model of hair-cell mechanotransduction
41 postulates that excitatory stimuli that deflect the bundle towards the tallest stereocilia will tension
42 the tip links, thereby transferring the mechanical force to the associated MET channel (Basu et al.,

43 2016; Corey and Hudspeth, 1983; Pickles et al., 1984). How the MET channel complex is assembled to
44 transduce mechanical stimuli is largely unknown.

45

46 Our current understanding is that the MET channel complex is composed of the tip link protein
47 PCDH15, and the multipass transmembrane proteins lipoma HMGIC fusion partner-like 5 (LHFPL5),
48 transmembrane inner ear (TMIE), and transmembrane channel-like proteins (TMC1/2) (Beurg et al.,
49 2015; Kawashima et al., 2011; Kurima et al., 2015; Maeda et al., 2014; Xiong et al., 2012; Zhao et al.,
50 2014). Although conclusive evidence is still lacking, the TMCs are currently the most promising
51 candidates for the pore-forming subunit of the MET channel (Corey and Holt, 2016; Wu and Muller,
52 2016). TMC proteins are present at the site of mechanotransduction at the stereocilia tips of hair
53 bundles (Beurg et al., 2015; Kurima et al., 2015), and can interact directly with PCDH15 (Beurg et al.,
54 2015; Maeda et al., 2014). In humans, mutations in *TMC1* are responsible for both recessive
55 (DFNB7/11) and dominant (DFNA36) forms of nonsyndromic deafness (Kurima et al., 2002). In mice,
56 *Tmc1/2* double knockouts have no conventional MET current (Kawashima et al., 2011). Several lines
57 of evidence support the idea that TMC1/2 are the candidate pore forming subunits of the MET
58 channel. Hair cells expressing either *TMC1* or *TMC2* alone exhibit MET channel properties that are
59 distinct from those observed when both proteins are present, suggesting the TMCs may form
60 heteromeric complexes (Pan et al., 2013). Consistent with this finding, the tonotopic gradient in MET
61 channel conductance of outer hair cells (OHCs) is eliminated in *Tmc1* KO mice (Beurg et al., 2014).
62 Moreover, the *Beethoven* (*Bth*) M412K amino acid change in mouse TMC1 reduces the calcium
63 permeability and conductance of the MET channel (Corns et al., 2016; Pan et al., 2013). For these
64 reasons, it is important to understand the role of TMC1/2 in mechanotransduction and how they form
65 a functional unit with other members of the MET complex.

66

67 The zebrafish *mercury* (*mrc*) mutant was originally identified in a forward genetic screen for genes
68 required for hearing and balance (Nicolson et al., 1998). Similar to those genes directly involved in
69 hair-cell mechanotransduction (*cdh23 / sputnik, pcdh15a / orbiter*), the *mercury* phenotype is
70 characterized by (i) balance defects, (ii) an absence of the acoustic startle reflex, (iii) failure to inflate
71 the swim bladder, (iv) lack of hair cell-dependent calcium responses in the hindbrain, and (v)
72 undetectable microphonic currents. Together, these phenotypes suggest that the *mercury* gene is
73 essential for hair-cell mechanotransduction.

74

75 Here we report that mutations in the zebrafish *transmembrane O-methyltransferase* (*tomt*) gene are
76 causative for the *mercury* mutant phenotype. The Tomt protein is predicted to have a S-
77 adenosylmethionine (SAM)- dependent methyltransferase domain that is most closely related to
78 Catechol O-methyltransferase (Comt; EC 2.1.1.6). The human ortholog of the *tomt* gene is called
79 Leucine Rich and O-Methyltransferase Containing (*LRTOMT*), a dual reading frame locus that codes
80 for either Leucine Rich Repeat Containing 51 (*LRTOMT1 / LRRC51*) or TOMT (*LRTOMT2*). Mutations
81 in *LRTOMT2* are responsible for DFNB63, a non-syndromic, autosomal recessive form of human
82 deafness that is characterized by severe to profound neurosensory hearing loss that can be
83 congenital or prelingual (Ahmed et al., 2008; Du et al., 2008; Kalay et al., 2007; Khan et al., 2007; Tlili
84 et al., 2007). No vestibular dysfunction has been described for DFNB63 patients. A mouse model of
85 DFNB63 has also been reported. The *add* mouse (named for its attention deficit disorder-like
86 symptoms) has a single R48L amino acid change in the *Tomt* (*Comt2*) gene, and behavioral analyses
87 confirm that TOMT is required for both auditory and vestibular function (Du et al., 2008). The major
88 findings from the mouse model of DFNB63 were that TOMT exhibits modest O-methyltransferase

89 activity towards the catecholamine norepinephrine, and that there is progressive degeneration of
90 cochlear hair cells in TOMT-deficient mice. Based on these findings, the authors speculated that the
91 hair-cell pathology was caused by deficient degradation of catecholamines. However, this hypothesis
92 has not been tested.

93

94 Using the *mercury* mutant zebrafish as a model of DFNB63, we have found that Tomt-deficient hair
95 cells have no mechanotransduction current. Mechanotransduction in *mercury* mutants can be rescued
96 by transgenic expression of either zebrafish Tomt or mouse TOMT, but not with the closely related
97 Comt enzyme. This result suggests that catecholamine metabolism is not the cause of the MET
98 defects. Instead, we show that Tomt is required for trafficking Tmc proteins to the hair bundle. We
99 find that GFP-tagged Tmc1 and Tmc2b fail to localize to the hair bundle in *mercury* mutants, and that
100 Tomt can rescue this trafficking defect. Furthermore, mouse TOMT and TMC1 can interact in HEK
101 293 cells, and this interaction is modulated by His183 in the putative active site of TOMT. Together,
102 these data suggest that DFNB63 is unlikely to be a disease involving catecholamine metabolism.
103 Rather, TOMT-deficient hair cells exhibit a specific defect in mechanotransduction that can be
104 explained by a failure of TMCs to properly localize to the hair bundle. As such, we propose a model
105 where a TOMT-TMC interaction is required in the secretory pathway of hair cells for the proper
106 integration of TMC proteins into the MET complex.

107

108

109 **Results**

110

111 **Identification of the *mercury* mutation**

112

113 The *mercury tk256c* locus (Nicolson et al., 1998) was initially mapped between the SSLP markers
 114 Z20009 (G₄1723) and Z858 (G₄0668) on the distal end of chromosome 15. Sequencing of known
 115 candidate genes within this region revealed no pathogenic mutations and mRNA *in situ* hybridization
 116 (ISH) for these genes did not reveal any transcripts with hair cell-enriched expression patterns (data
 117 not shown). To determine if there were any genes within the *mercury* critical region that were not
 118 annotated in the zebrafish genome assembly, we identified a region with conserved synteny on the
 119 stickleback (*Gasterosteus aculeatus*) group1 chromosome that contained many of the *mercury*
 120 candidate genes previously excluded by sequencing and ISH, including *inpp1a*, *stard10*, *clpb*, *phox2a*,
 121 and the folate receptor *IZUMO1R* (Assembly BROAD S1 - group1:6160000-6236000). The stickleback
 122 ortholog of the human deafness gene *LRTOMT / DFNB63* was also present in this region (*tomt*,
 123 ENSGACG00000007832). We used the stickleback Tomt protein sequence to identify *tomt*-positive
 124 contigs in the Sanger database of *de novo* zebrafish genome assemblies derived from Illumina
 125 sequencing of AB and TU double haploid individuals ([http://www.sanger.ac.uk/cgi-](http://www.sanger.ac.uk/cgi-bin/blast/submitblast/d_rerio)
 126 [bin/blast/submitblast/d_rerio](http://www.sanger.ac.uk/cgi-bin/blast/submitblast/d_rerio)) (Table 1). Using this information, we cloned and sequenced the
 127 zebrafish *tomt* open reading frame from larval RNA (Accession number KX066099). Additionally, we
 128 amplified and sequenced each of the three coding exons and their flanking intronic regions from
 129 genomic DNA, and found that each *mercury* allele contains a nonsense mutation in the first exon of
 130 *tomt* (Figure 1A). These mutations truncate the protein product prior to (*tk256c*) or early within (*nl16*)
 131 the putative O-methyltransferase domain (Figure 1B), and are both predicted to be functional nulls.

Table 1.

Sanger AB and Tuebingen *de novo* genomic assembly contigs containing *tomt* coding sequence (GenBank: KX066099)

AB strain (DHAB) Illumina <i>de novo</i> assembly		
Contig Name	Exon	Region of <i>tomt</i> CDS
Contig_000336392	1	1-262

Contig_000381119	2	263-459
Contig_000235950	3	460-780

Tuebingen strain (DHTu2) Illumina *de novo* assembly

Contig Name	Exon	Region of <i>tomt</i> CDS
c306000518.Contig1	1	1-60
c279701478.Contig1	1	1-258
c280900030.Contig1	1	141-262
c301500577.Contig1	2	263-459
c282600514.Contig1	3	730-780
c282201256.Contig1	3	460-780
c008000433.Contig1	3	460-599

132

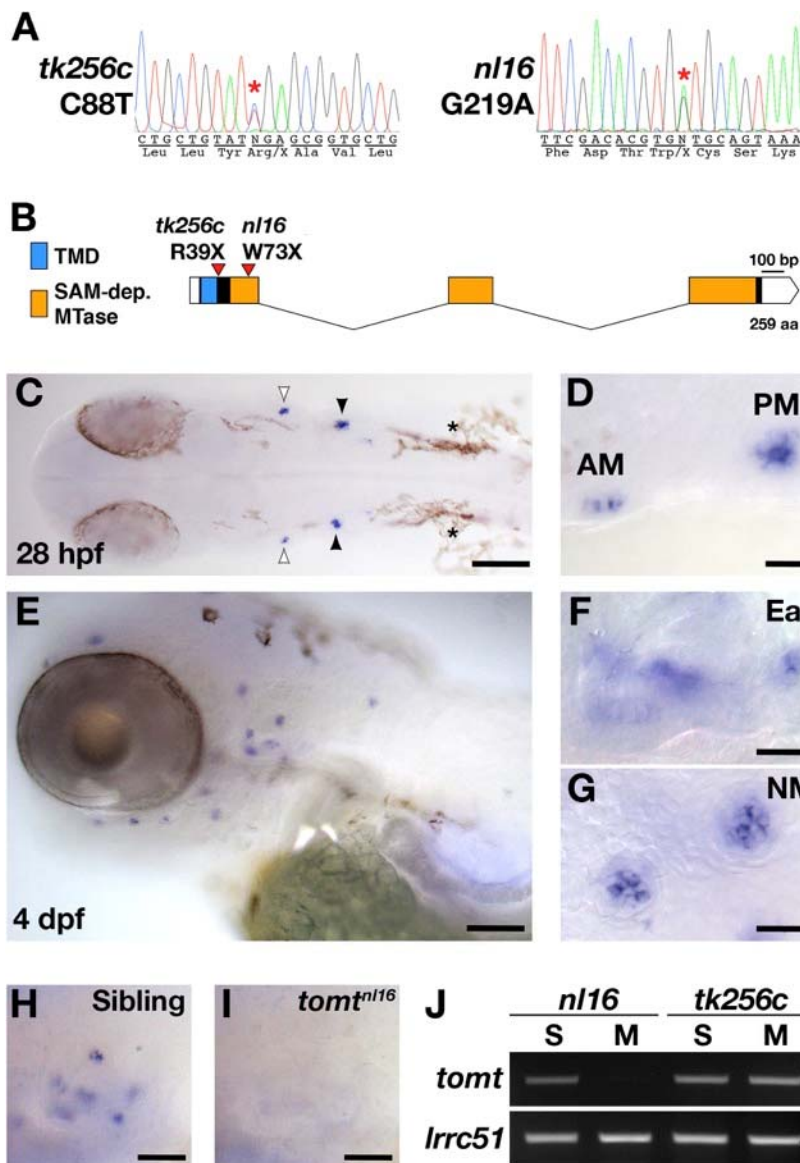


Figure 1. *mercury* mutations and *tomt* mRNA expression. **A** – Representative chromatograms from heterozygous *mercury* mutants showing the C88T and G219A mutations for the *tk256c* and *nl16* alleles respectively. **B** – Diagram of the predicted exon-intron structure for the *tomt* gene. Regions coding for the putative transmembrane domain (TMD, blue) and SAM-dependent O-methyltransferase domain (SAM-dep. MTase, orange) are shown, along with the positions of the *tomt*^{*tk256c*} R39X and *tomt*^{*nl16*} W73X mutations. **C-G** – Whole mount mRNA *in situ* hybridization (ISH) for *tomt* in 28 hours post-fertilization (hpf) (C, D) and 4 days post-fertilization (dpf) (E-G) zebrafish

153 larva. **C** – At 28 hpf, *tomt* is expressed in exclusively in the presumptive anterior (AM) and posterior
 154 (PM) maculae of the developing ear, as indicated by the white and black arrow heads respectively.
 155 Pigment cells are indicated by asterisks (*). The embryo is shown in dorsal view with anterior to the
 156 left. **D** – A close up of the AM and PM from the larva in C. **E-G** – At 4 dpf, *tomt* is expressed exclusively
 157 in the hair cells of the inner ear (F) and lateral line neuromasts (G). Larva is shown in lateral view with
 158 anterior to the left and dorsal at the top. **H, I** – ISH for *tomt* in a *tomt*^{*nl16*} WT sibling (H) and mutant (I)
 159 at 4 dpf. Inner ear sensory patches are shown. **J** – RT-PCR for *tomt* and *lrrc51* from total RNA isolated
 160 from 5 dpf *tomt*^{*nl16*} and *tomt*^{*tk256c*} siblings (S) and mutants (M). Scale bars: 100 μ m in C and E, 25 μ m in
 161 D, F and G, 50 μ m in F and G.

162 **Zebrafish *tomt* is expressed exclusively in hair cells**

163

164 To determine where the *tomt* gene is expressed, we performed whole mount mRNA ISH using the
165 *tomt* coding sequence as a probe. At 28 hours post-fertilization (hpf), we observed ISH signal
166 exclusively in the hair cells of the anterior and posterior maculae in the developing ear (Figure 1C, D).
167 At 4 days post-fertilization (dpf), *tomt* is expressed specifically in hair cells of the inner ear and lateral
168 line organ (Figure 1E-G). We found that the ISH signal is absent in *tomt*^{nl16} mutants, suggesting that
169 the G219A mutation causes nonsense-mediated mRNA decay (inner ear shown - Figure 1H, I). This
170 result was confirmed using RT-PCR (Figure 1J). We were unable to amplify the *tomt* transcript from
171 total RNA of homozygous *tomt*^{nl16} mutants, but were still able to detect it in *tomt*^{tk256c} mutants.
172 *lrrc51*, the gene that codes for the LRTOMT1 protein in humans, was used as a control.

173

174 **Tomt is enriched in the Golgi apparatus**

175

176 *tomt* is predicted to code for a single-pass membrane protein featuring a short N-terminus followed
177 by a transmembrane domain (TMD), with approximately 20 amino acids separating the TMD from
178 the predicted O-methyltransferase catalytic domain. Immunolabel of TOMT in mouse cochlear hair
179 cells localized the protein in the cytoplasm of inner and outer hair cells, and showed enrichment
180 below the cuticular plate of OHCs (Ahmed et al., 2008). To determine the subcellular localization of
181 Tomt in zebrafish hair cells, we used the hair cell-specific promoter *myo6b* to mosaically express
182 Tomt tagged with either GFP or an HA epitope at its C-terminus. Both Tomt-GFP and Tomt-HA are
183 enriched in an apical membrane compartment above the nucleus (Figure 2A, B), similar to
184 immunostain for mouse TOMT. Notably, no Tomt protein is detectable in the hair bundle.

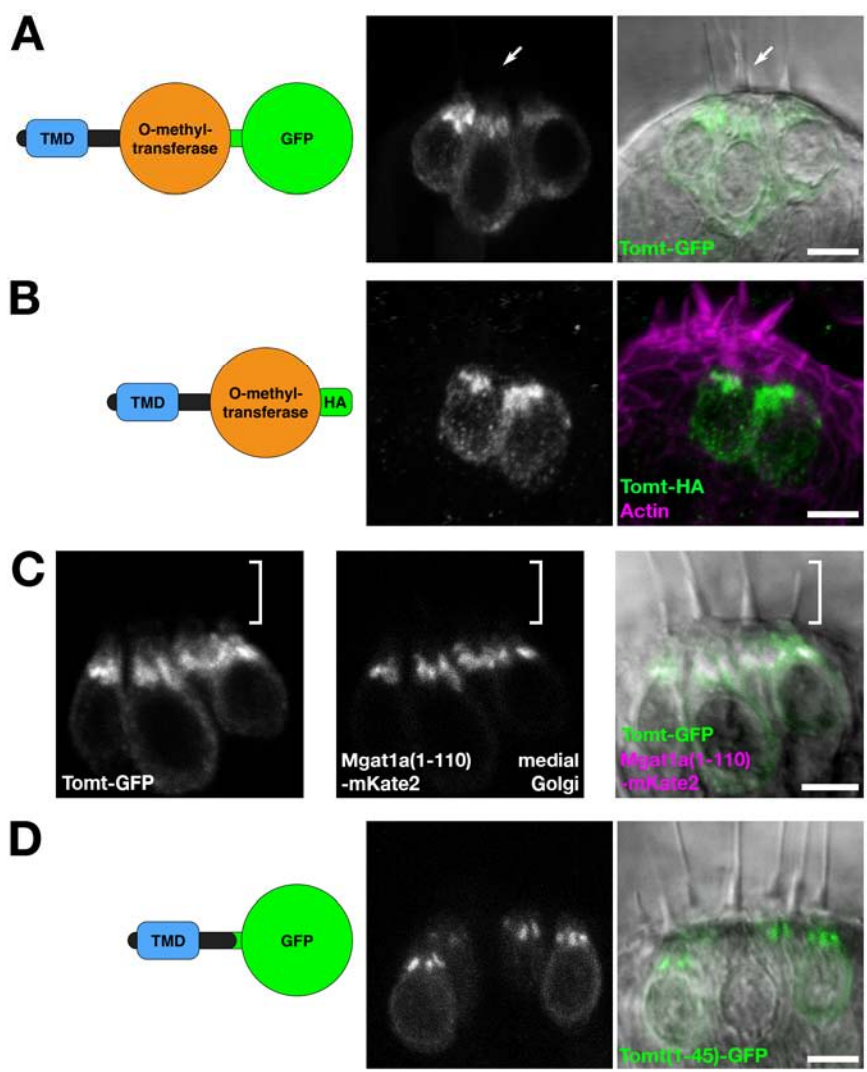
185

186 In hair cells, the Golgi apparatus is positioned apical to the nucleus (Sipe et al., 2013). To confirm that
187 the Tomt-enriched compartment is within the Golgi apparatus, we engineered a medial Golgi marker
188 by fusing the first 110 amino acids of the zebrafish glycosyltransferase Mgat1a (*mannosyl (alpha-1,3-*
189 *)glycoprotein beta-1,2-N-acetylglucosaminyltransferase a*) to the mKate2 far-red fluorescent protein
190 (Mgat1a(1-110)-mKate2). This portion of Mgat1a includes the TMD and stem regions of the protein,
191 and previous studies have shown that these regions are necessary and sufficient for localization and
192 retention in the medial Golgi cisternae (Tu and Banfield, 2010). When co-expressed, Tomt-GFP and
193 Mgat1a(1-110)-mKate2 are partially co-localized in hair cells (Figure 2C). Compared to Mgat1a(1-
194 110)-mKate2, Tomt-GFP is more broadly distributed indicating that Tomt-GFP may be present at
195 lower levels in the endoplasmic reticulum and the basolateral membrane in addition to the Golgi
196 apparatus.

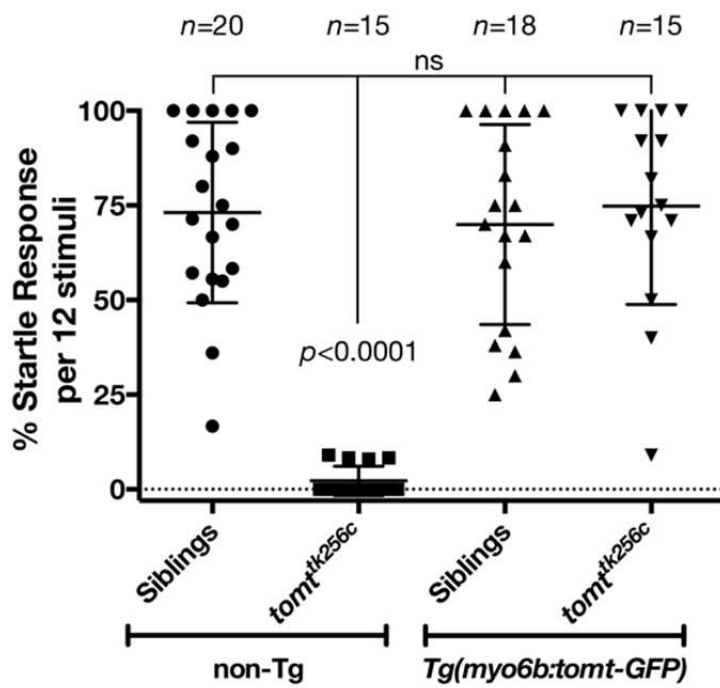
197

198 We noted that the organization of Tomt's predicted protein domains was reminiscent of Golgi-
199 resident, Type II transmembrane glycosyltransferases like Mgat1- a short N-terminus followed by a
200 signal anchor TMD, and a stem region preceding the catalytic domain (Tu and Banfield, 2010). To
201 test if the putative TMD and stem regions of Tomt are required for its localization, we expressed the
202 first 45 amino acids of Tomt C-terminally tagged with GFP. Similar to Tomt-GFP and Tomt-HA,
203 Tomt(1-45)-GFP is also enriched in the Golgi apparatus (Figure 2D). Together, these results suggest
204 that Tomt is a Golgi-enriched protein, and that the first 45 amino acids of Tomt are sufficient for its
205 subcellular localization.

206



207
 208 **Figure 2.** Tomt protein localization. **A** – Diagram of the protein made from the *Tg(myo6b:tomt-GFP)*
 209 transgene plus an image of Tomt-GFP localization in live hair cells of the anterior crista in the inner
 210 ear at 3 dpf. **B** – Diagram of the protein made from the *Tg(myo6b:tomt-HA)* transgene plus
 211 immunolabel for the HA epitope showing Tomt-HA localization in the hair cells of the anterior crista
 212 in the inner ear at 4 dpf. Phalloidin stain (magenta) marks F-Actin. **C** – Co-localization between Tomt-
 213 GFP and a medial Golgi marker (Mgat1a_1-110-mKate2) in live hair cells of the lateral crista (3 dpf). **D**
 214 – Diagram of the protein made from the *Tg(myo6b:tomt_1-45-GFP)* transgene plus an image of
 215 Tomt_1-45-GFP localization in live hair cells of the lateral crista at 4 dpf. Scale bars: 5 μm in A-D.
 216



217
218

219 **Figure 3.** Auditory Evoked Behavior Response (AEBR) in 6 dpf *tomt^{tk256c}* siblings and mutants, with or
 220 without the *myo6b:tomt-GFP* transgene. The genotype of each group is labeled below, and the
 221 number of individuals analyzed for each genotype shown above. Each data point represents the
 222 percent of startle responses per trial of 12 stimuli for an individual larva. Error bars show the mean +/-
 223 SD. Statistical comparisons were made by one-way ANOVA with Bonferroni's multiple comparison
 224 test.

225 **Hearing loss is rescued by Tomt-GFP in *mercury* mutants**

226

227 To confirm that mutations in *tomt* are responsible for the *mercury* phenotype, and show that the

228 Golgi-enriched Tomt-GFP was functional, we asked whether the *myo6b:tomt-GFP* (*Tg(tomt)*)

229 transgene could rescue the Acoustic Evoked Behavior Response (AEBR) in 6 dpf *tomt*^{tk256c} mutants

230 (Figure 3). On average, wild-type, non-transgenic siblings responded to 72% of the acoustic stimuli (*n*

231 = 20, 138/192 stimulations). In contrast, non-transgenic *mercury* mutants exhibited a startle response

232 to 2% of stimuli, confirming that Tomt-deficient zebrafish are deaf (*n* = 15; 4/177 stimulations).

233 Strikingly, we were able to restore full auditory function to *mercury* mutants with the *tomt-GFP*

234 transgene. The AEBR of *Tg(tomt); tomt*^{tk256} larvae (*n* = 15; 118/158 stimulations) was statistically

235 indistinguishable from wild-type, non-Tg and wild-type *Tg(tomt)* larvae (*n* = 18; 128/183 stimulations).

236 These data confirm that *tomt* is the gene responsible for the *mercury* phenotype and indicate that the

237 Golgi-enriched Tomt-GFP protein is fully functional and can rescue the behavioral phenotype of

238 *mercury* mutants.

239

240 **Tomt is required for mechanotransduction in hair cells**

241

242 The initial characterization of the *mercury* mutant suggested that the auditory and vestibular deficits

243 were due to a lack of hair-cell mechanotransduction. The lateral line hair cells of *mercury* mutants

244 lack microphonic currents and FM 1-43 dye uptake, both phenotypes associated with

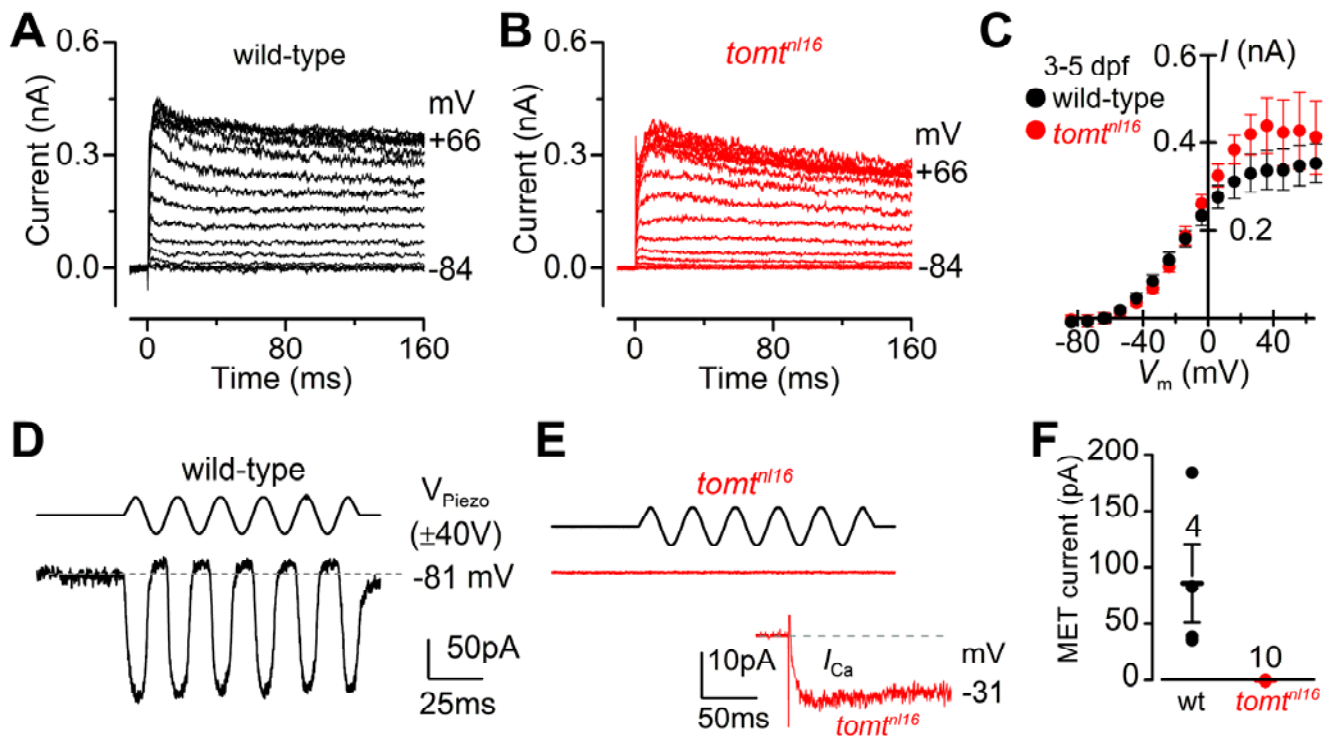
245 mechanotransduction defects (Nicolson et al., 1998; Seiler and Nicolson, 1999). To confirm whether

246 Tomt-deficient hair cells have a specific defect in mechanotransduction, we performed

247 electrophysiological recordings from lateral-line hair cells in wild-type and *mercury* mutants. Hair

248 cells from the lateral line organ of wild-type and *tomt*^{nl16} mutant zebrafish (3.0 - 5.2 dpf) showed a

249 similar complement of K^+ currents (Figure 4A, B), in agreement with that previously described for
 250 wild-type hair cells (Olt et al., 2016, 2014). The size of the peak K^+ current measured at 0 mV was
 251 found to be similar between wild-type (261 ± 26 pA, $n = 4$) and mutant hair cells (352 ± 43 pA, $n = 3$)
 252 (Figure 4C). We then investigated whether the mechanoelectrical transducer (MET) current was
 253 affected in *Tomt*-deficient hair cells from 4.0 - 5.2 dpf zebrafish (Figure 4D-F). MET currents were
 254 elicited at the holding potential of -81 mV while displacing the hair bundles with sine wave stimuli
 255 from a piezoelectric-driven fluid jet (Corns et al., 2016, 2014). In wild-type hair cells, the size of the
 256 MET current was 86 ± 35 pA ($n = 4$ from 4 zebrafish, Figure 4D, F), with a resting open probability of
 257 the MET channel of 0.08 ± 0.03 ($n = 4$). By contrast, *Tomt*-deficient hair cells have no detectable MET
 258 current ($n = 10$ from 6 zebrafish; Figure 4E, F). The presence of the inward Ca^{2+} current (inset in Figure
 259 4E) was used to confirm hair cell-identity in *tomt*^{nl16} mutants. The peak of the Ca^{2+} current at -31 mV
 260 was 9.2 ± 2.4 pA ($n = 8$), which was similar to that previously reported (Olt et al., 2016).



261
 262

263 **Figure 4.** Tomt-deficient hair cells have no mechanotransduction (MET) current. **A, B** – Examples of
264 K^+ currents recorded from lateral line hair cells in wild-type sibling (A) and *tomt^{nl16}* mutant (B)
265 zebrafish. Currents were elicited by depolarizing and hyperpolarizing voltage steps in 10 mV nominal
266 increments from the holding potential of -84 mV. **C** – Average peak current-voltage (*I-V*) curves from
267 hair cells in wild-type ($n = 4$) and *tomt^{nl16}* mutant ($n = 3$) hair cells, including those in panels A and B.
268 **D, E** – Saturating MET currents in 4 dpf zebrafish recorded from wild-type (**D**) and *tomt^{nl16}* mutant (**E**)
269 lateral line hair cells in response to a 50 Hz sinusoidal force stimulus to the hair bundles at the
270 membrane potential of -81 mV, which is indicated by the dashed line (**D**). V_{Piezo} indicates the driver
271 voltage to the fluid jet, with positive deflections moving the hair bundles in the excitatory direction.
272 Note the absence of the MET current in the *tomt^{nl16}* mutant hair cell (**E**). The inset in panel **E** shows
273 the calcium current recorded from the same cell in response to 150 ms depolarizing voltage steps in
274 10 mV increments from the holding potential of -81 mV. For clarity, only the peak Ca^{2+} current trace
275 at -31 mV is shown. **F** – Average maximum MET current in both wild-type (wt) and mutant (*tomt^{nl16}*)
276 hair cells. Mean values in this Figure and text are quoted as means \pm S.E.M.
277

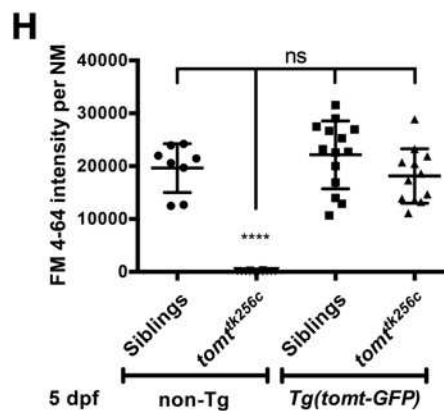
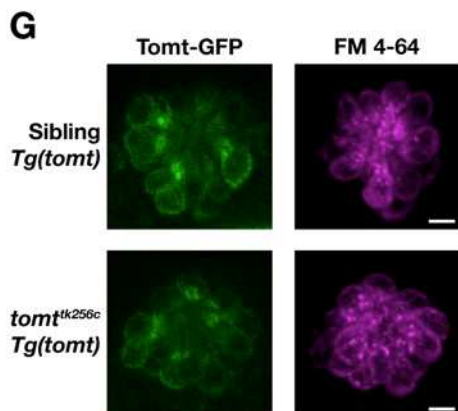
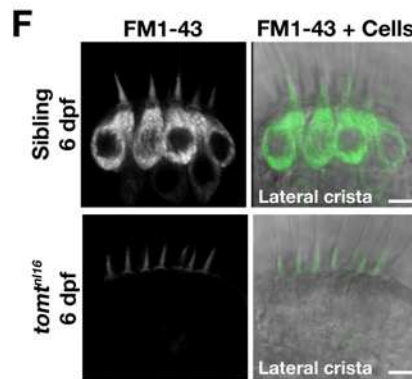
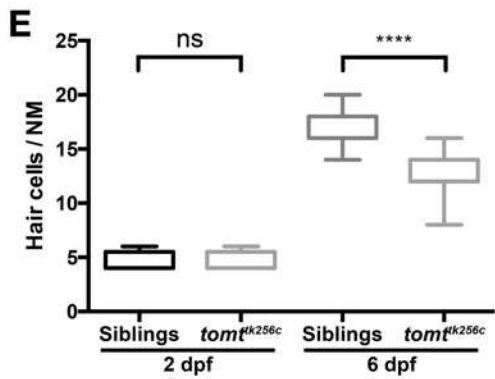
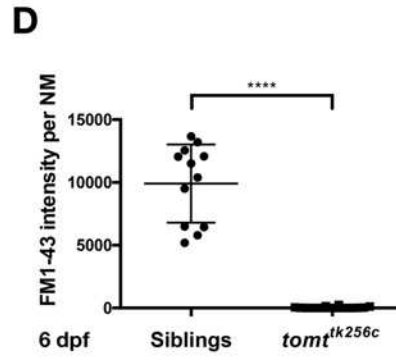
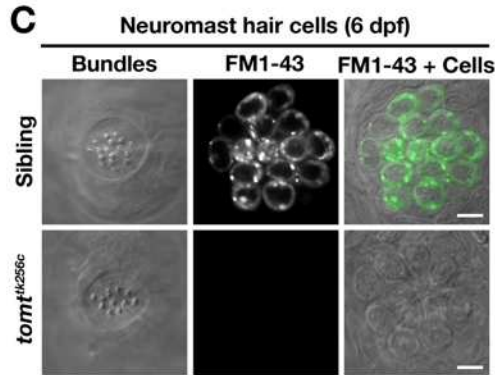
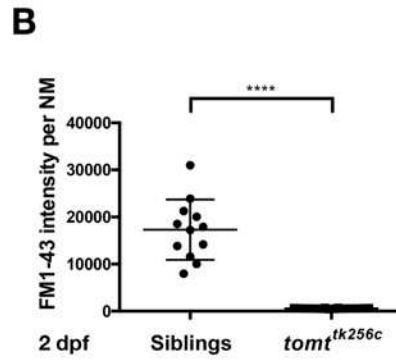
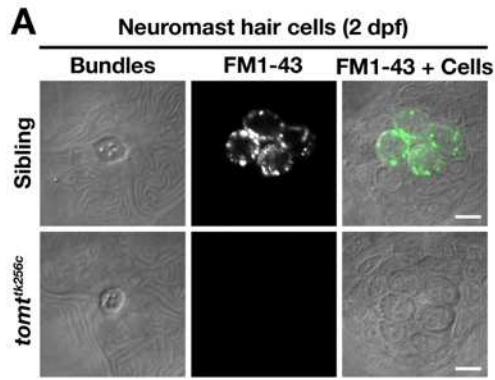
278 We confirmed the absence of a functional MET channel in Tomt-deficient hair cells by using the styryl
279 fluorescent dyes FM 1-43 and FM 4-64. These dyes are known to rapidly enter hair cells through MET
280 channels, thereby serving as a visual assay for basal channel activity (Gale et al., 2000; Meyers et al.,
281 2003; Nishikawa and Sasaki, 1996; Seiler and Nicolson, 1999). Nascent hair cells of the lateral line
282 organ will begin to label with FM dyes at 2 dpf (Figure 5A; $n = 6$ individuals, 2 NM each) (Kindt et al.,
283 2012). However, Tomt-deficient hair cells did not label with FM 1-43 at this early developmental
284 stage ($n = 8$ individuals, 2 NM each; Figure 5A, B), even though the neuromasts from *tomt*^{tk256c}
285 mutants contained the same number of hair cells (Figure 5E). To show that the lack of functional MET
286 channels was not a case of developmental delay, we also quantified FM 1-43 uptake at 6 dpf, a stage
287 when wild-type neuromasts contain an average of 17 hair cells per neuromast ($n = 6$ individuals, 2 NM
288 each; Figure 5C-E). At 6 dpf, Tomt-deficient hair cells still did not label with FM 1-43 (Figure 5C, D). At
289 this stage, we observed a significant decrease in the number of hair cells per neuromast in *mercury*
290 mutants (Figure 5E, average of 13 HC / NM; $n = 8$ individuals, 2 NM each), consistent with what has
291 been observed in other zebrafish mechanotransduction mutants (Seiler et al., 2005). The auditory
292 and vestibular phenotypes of *mercury* mutants suggest that the hair cells of the inner ear also have
293 defects in mechanotransduction. Injecting FM 1-43 into the ear of 6 dpf wild-type larvae led to robust
294 labeling of inner ear hair cells (Figure 5F, top, lateral cristae shown, $n = 5$). However, like the lateral
295 line organ, Tomt-deficient inner ear hair cells failed to label with FM 1-43 dye ($n = 7$). We did not
296 observe any gross polarity (Figure 5 – figure supplement 1A, B) or morphological defects (Figure 5 –
297 figure supplement 1C-E) that could account for the lack of MET channel activity in the *mercury*
298 mutant. Together with the electrophysiological recordings in Figure 4, these data demonstrate that
299 Tomt-deficient hair cells lack functional MET channels, even during the initial development of
300 mechanosensitivity.

301

302 **Tomt-GFP can restore MET channel activity to *mercury* mutants**

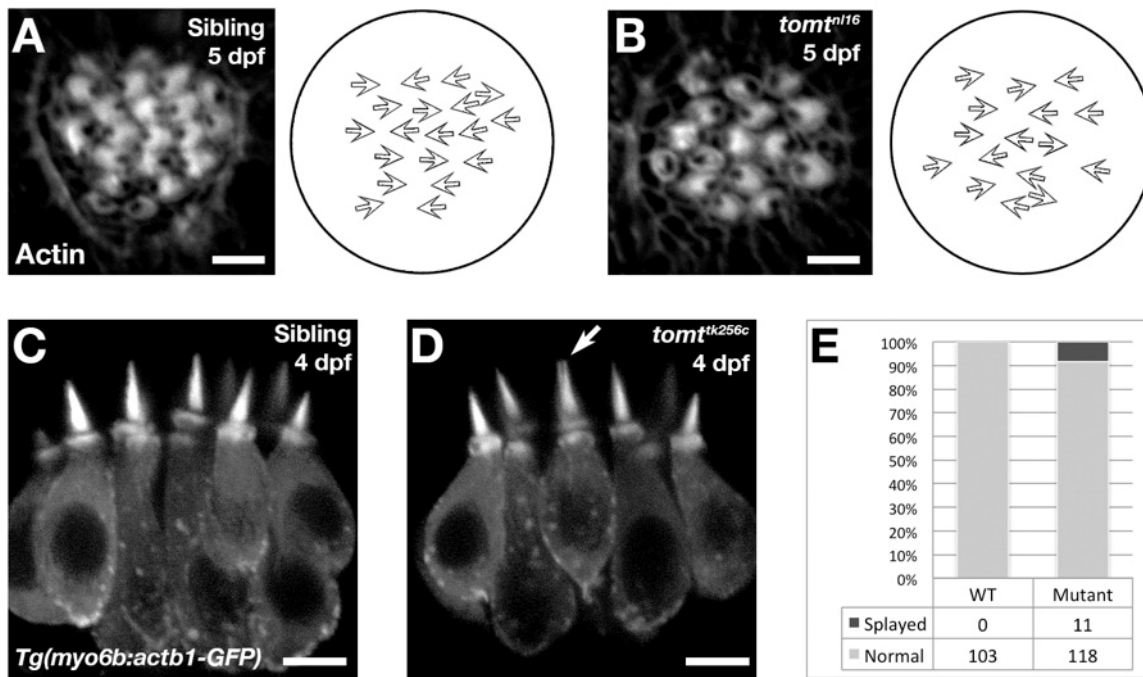
303 Having established that we could rescue the deafness phenotype in *mercury* mutants with the *tomt-*
304 *GFP* transgene (Figure 3), we then assayed for FM dye labeling in lateral line hair cells to determine
305 whether Tomt-GFP could rescue the mechanotransduction defect. We observed that FM 4-64 label
306 in wild-type *Tg(tomt)* neuromasts was statistically identical to their wild-type, non-transgenic
307 counterparts (Figure 5G, H), indicating that extra Tomt protein does not appreciably alter the basal
308 function of the MET channel. The lack of FM label was fully rescued in mutants stably expressing the
309 *tomt-GFP* transgene specifically in hair cells (Figure 5G, H). We also observed full rescue of FM dye
310 labeling in a transgenic line expressing Tomt-HA (*Tg(myo6b:tomt-HA-pA)*; Figure 5 – figure
311 supplement 2A). In contrast, we were unable to rescue FM 4-64 label using a cytoplasmic form of
312 Tomt (HA-Tomt(45-259)-GFP), modeled after human S-COMT (Accession # NP_009294) (Figure 5 –
313 figure supplement 2B, C), suggesting that the Golgi-targeting sequence is required for Tomt
314 function. Conversely, the putative enzymatic portion of Tomt is also required for rescue, as Tomt(1-
315 45)-GFP also had no effect on FM 4-64 label in wild-type or *mercury* mutants (Figure 5 – figure
316 supplement 2D-F). These data suggest that Tomt is necessary for mechanotransduction in sensory
317 hair cells, and that both the Golgi-targeting sequence and putative enzymatic domains are required.

318



319
320

321 **Figure 5.** Tomt-deficient hair cells do not label with MET-channel permeant FM dyes. **A-D** – FM 1-43
322 dye label of lateral line hair cells in 2 dpf (A, B) and 6 dpf (C, D) wild-type siblings and *tomt*^{tk256c}
323 mutants. **A, C** – Representative DIC images of NM hair bundles (left), fluorescence images of FM 1-43
324 in the same NMs (middle), and a merge of the FM 1-43 images with DIC images of the hair cell bodies
325 (right) from 2 dpf (A) and 6 dpf (C) wild-type siblings and *tomt*^{tk256c} mutants. **B, D** – Quantification of
326 FM 1-43 fluorescence intensity per NM of 2 dpf (B) and 6 dpf (D) wild-type siblings (*n* = 6 larvae; 2
327 NMs each) and *tomt*^{tk256c} mutants (*n* = 8 larvae; 2 NMs each). Error bars are the mean +/- SD.
328 Asterisks indicate *p* < 0.0001 by unpaired, two-tailed t-test. **E** – Quantification of hair cell number per
329 neuromast in 2 dpf and 6 dpf *tomt*^{tk256c} mutants and wild-type siblings (same as those shown in
330 panels A – D). The box plots cover the 25th to 75th percentiles, and the whiskers represent the
331 minimum and maximum counts. ns = not significant, asterisks indicate *p* < 0.0001 by unpaired, two-
332 tailed t-test. **F** – Representative images of FM 1-43 labeling of inner ear hair cells in 6 dpf wild-type
333 siblings (*n* = 5 larvae) and *tomt*^{nl16} mutants (*n* = 7 larvae). **G** – Rescue of FM dye labelling in *mercury*
334 mutants by stably expressed Tomt-GFP. Representative images of Tomt-GFP (left panels) and FM 4-
335 64 (right panels) in lateral line NMs of a *Tg(myo6b:tomt-GFP)* wild-type sibling and a *Tg(myo6b:tomt-*
336 *GFP);tomt*^{tk256c} mutants at 5 dpf. Tomt-GFP and FM 4-64 images are from the same NM for each
337 genotype. **H** – Quantification of FM 4-64 fluorescence intensity per NM for 5 dpf non-transgenic wild-
338 type siblings (*n* = 6 larvae, 8 NMs), non-transgenic *tomt*^{tk256c} mutants (*n* = 6 larvae, 12 NMs),
339 *Tg(myo6b:tomt-GFP)* wild-type siblings (*n* = 7 larvae, 14 NMs), and *Tg(myo6b:tomt-GFP);tomt*^{tk256c}
340 mutants (*n* = 6 larvae, 12 NMs), including those NMs shown in F. Error bars are the mean +/- SD. ns =
341 not significant. Asterisks indicate *p* < 0.0001 by one-way ANOVA with Bonferroni's multiple
342 comparison test. Scale bars: 5 μm in A, C, F, and G.
343

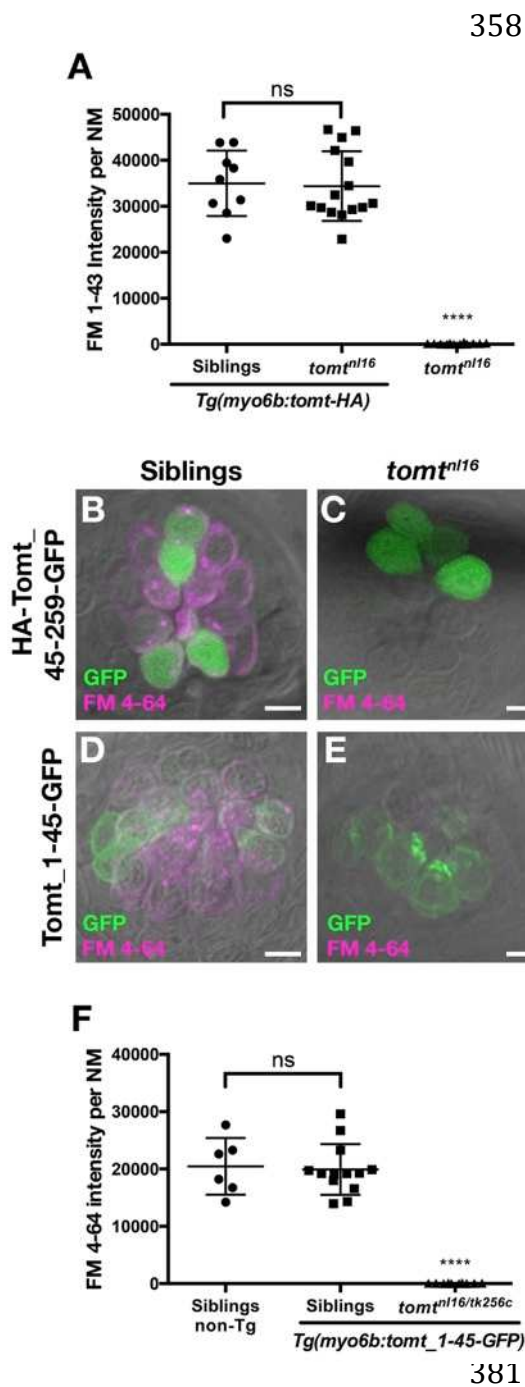


344
345

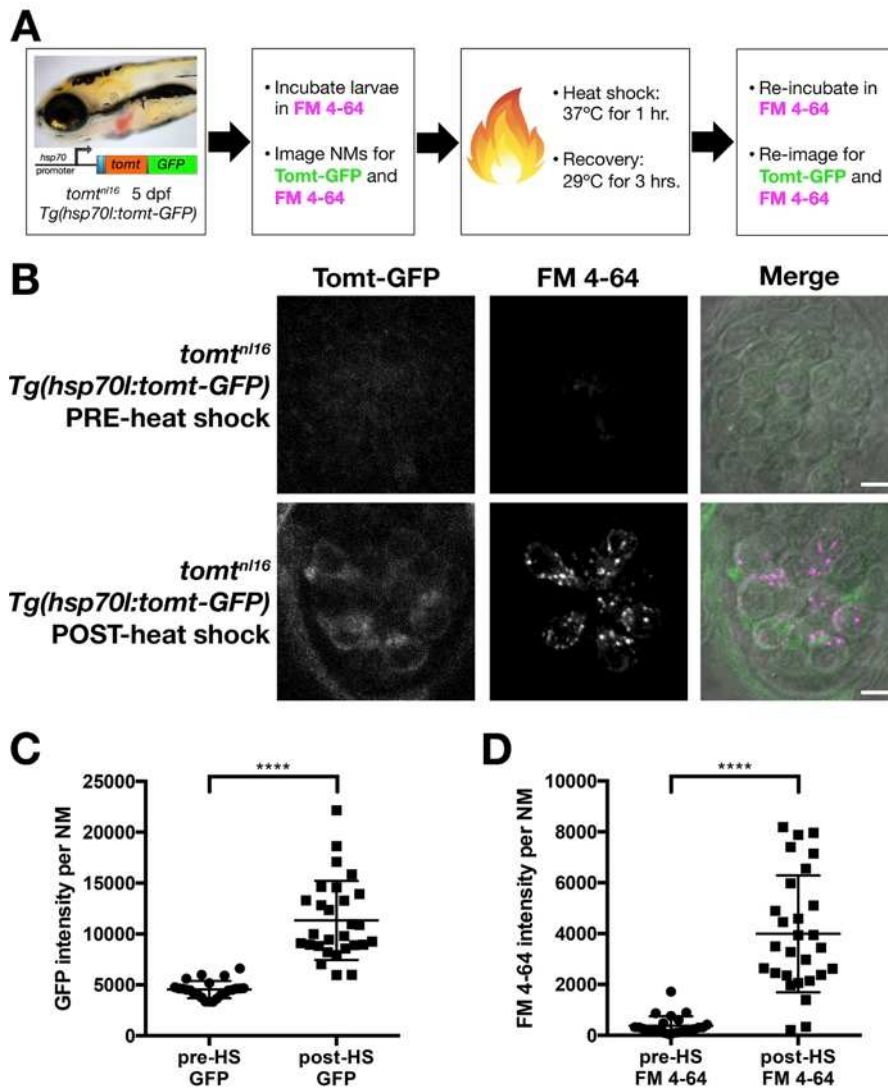
346 **Figure 5 – figure supplement 1. A, B** –Hair cell planar polarity in neuromasts of *mercury* mutants.
 347 Images of hair bundles from 5 dpf wild-type sibling (B) and *tomt^{nl6}* mutant (C) larvae stained with
 348 phalloidin-488 for F-Actin. Accompanying each image is a diagram of the planar polarity of each hair
 349 bundle. **C-E** – Inner ear hair cell morphology in *mercury* mutants. **C, D** - Representative images of hair
 350 cells in lateral cristae expressing β actin-GFP from *Tg(myo6b:actb1-GFP)* wild-type siblings (D) and
 351 *tomt^{tk256c}* mutants (E) at 4 dpf. White arrow indicates a splayed hair bundle sometimes observed in
 352 *mercury* mutants. **E** – Quantification of the splayed bundle phenotype in wild-type siblings ($n = 6$
 353 larvae, 103 lateral crista hair bundles), and *tomt^{tk256c}* mutants ($n = 8$ larvae, 129 lateral crista hair
 354 bundles). Scale bars = 3 μ m in B and C, 5 μ m in D and E.

355

356 **Figure 5 – figure supplement 2. A** – Tomt-HA can restore basal MET channel activity to *mercury*
 357 mutant hair cells. Quantification of FM 1-43 fluorescence intensity per NM for 5 dpf *Tg(myo6b:tomt-*



358 *HA)* siblings ($n = 3$ larvae, 9 NM) and *tomt^{nl16}* mutants ($n =$
 359 5 larvae, 15 NM), as well as non-transgenic *tomt^{nl16}*
 360 mutants ($n = 4$ larvae, 12 NM). Error bars are the mean \pm SD. ns = not significant. Asterisks indicate $p < 0.0001$ by
 361 one-way ANOVA with Bonferroni's multiple comparison
 362 test. **B, C** – Representative images of neuromasts from 4
 363 dpf wild-type (B) and *tomt^{nl16}* larvae transiently
 364 expressing a cytoplasmic form of Tomt (HA-Tomt_45-
 365 259-GFP). Cytoplasmic Tomt fails to rescue FM 4-64 label
 366 in *mercury* mutants ($n = 7$ individuals). **D, E** –
 367 Representative images of neuromasts from 4 dpf wild-
 368 type (D) and *tomt^{nl16}* larvae transiently expressing a form
 369 of Tomt lacking the putative enzymatic domain (Tomt_1-
 370 45-GFP). Transiently expressed Tomt_1-45-GFP fails to
 371 rescue FM 4-64 label in *mercury* mutants ($n = 2$). **F** –
 372 Quantification of FM 4-64 fluorescence intensity per NM
 373 in 4 dpf stable *Tg(myo6b:tomt_1-45-GFP)* wild-type
 374 siblings ($n = 6$ larvae, 13 NM) and *tomt^{nl16/tk256c}* compound
 375 mutants ($n = 4$ larvae, 10 NM), as well as non-transgenic
 376 wild-type siblings ($n = 2$ larvae, 6 NM). Error bars are the
 377 mean \pm SD. ns = not significant, asterisks indicate $p <$
 378 0.0001 by one-way ANOVA with Bonferroni's multiple
 379 comparison test. Scale bars = 5 μ m in B-E.



382

383 **Figure 6.** Restoration of MET channel activity in *mercury* mutant hair cells with heat shock-inducible
 384 Tomt-GFP. **A** – Workflow for the heat-shock inducible *tomt-GFP* transgene experiment. **B** –
 385 Representative images of Tomt-GFP (left panels), FM 4-64 (middle panels) and merged GFP, FM 4-64
 386 and DIC channels (right panels) in lateral line NMs of 5 dpf *Tg(hsp70:tomt-GFP); tomt^{nl16}* larvae pre-
 387 and post-heat shock. **C, D** – Quantification of GFP intensity (C) and FM 4-64 intensity (D) per NM of
 388 *Tg(hsp70:tomt-GFP); tomt^{nl16}* larvae ($n = 6$) pre- and post-heat shock. Error bars are the mean +/- SD.
 389 Asterisks indicate $p < 0.0001$ by unpaired, two-tailed t-test. Scale bars: 5 μm in B.

390

391 **Heat-shock inducible Tomt-GFP can restore MET channel activity to mature *mercury* mutant hair**
392 **cells**

393
394 The *myosin6b* promoter is active at all stages of zebrafish hair cell development (Kindt et al., 2012;
395 Seiler et al., 2004). As such, rescue by the *myo6b:tomt-GFP* transgene does not address whether
396 Tomt is actively required after hair cell maturation for normal MET channel activity. To supply Tomt
397 protein to *mercury* mutant hair cells post-development, we used a heat shock inducible approach
398 (Figure 6A). We chose a 5 dpf time point because the majority of neuromast hair cells are functionally
399 mature by this time (Kindt et al., 2012), thereby allowing us to determine if transient expression of
400 Tomt can restore MET to mutant hair cells that have developed without mechanotransduction.

401
402 Prior to heat shock treatment, no distinct Tomt-GFP signal was observed (Figure 6B, C), and little to
403 no FM 4-64 hair cell label could be detected (Figure 6B, D). Post-heat shock, we observed a
404 significant induction of Tomt-GFP and a significant increase in FM 4-64 intensity ($p < 0.0001$; Figure
405 6C, D). These results demonstrate that an acute pulse of Tomt-GFP can restore MET channel activity
406 to previously silent hair cells, and can do so within four hours of initiating the heat shock treatment.
407 As such, these data suggest that Tomt plays an active role in MET channel function.

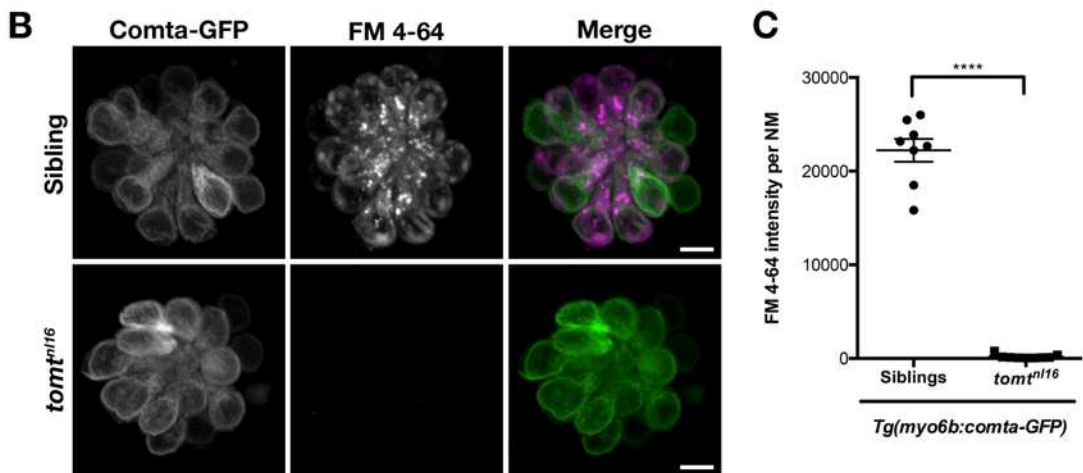
408
409 **Catechol-O-methyltransferase (Comt) cannot rescue mechanotransduction channel activity in**
410 ***mercury* mutants**

411
412 Tomt is classed together with Catechol O-methyltransferase (COMT) in the EC 2.1.1.6 catechol O-
413 methyltransferase protein family (UniProt Consortium, 2015). In their enzymatic domains, *Danio*
414 Tomt (amino acids 43-259, Accession # ANO40802) is 44% identical and 68% similar to human S-

415 COMT (Accession # NP_009294, amino acids 2-221) (Figure 7A). A previous study found that mouse
416 TOMT exhibited some catecholamine O-methyltransferase activity *in vitro* (Du et al., 2008). Based on
417 these data, it was speculated that TOMT acts as a catechol O-methyltransferase *in vivo*, and that the
418 deafness phenotype of the mouse mutant was caused by hair-cell degeneration resulting from a
419 failure to properly metabolize catecholamines. If the *mercury* phenotype were caused by excess
420 catecholamine, one would predict that increasing Comt activity would rescue mechanotransduction
421 in Tomt-deficient hair cells. To test this hypothesis, we created a stable transgenic line expressing
422 the zebrafish *comta* gene fused to GFP under the control of the hair cell specific *myo6b* promoter -
423 *Tg(myo6b:comta-GFP)*. Homozygous *mercury* larvae expressing Comta-GFP exhibited auditory and
424 vestibular defects identical to non-transgenic mutants (data not shown), and Comta-GFP had no
425 effect on FM 4-64 label in Tomt-deficient hair cells (Figure 7B, C). These results suggest that deficient
426 catecholamine metabolism in hair cells is not the cause of the *mercury* phenotype.
427

A

Human S-COMT	2	GDTKEQRILNHLVQHAEPGNAQSVLEAIDTYCEQKEWANNVGDKKGIKIVDAVIOEHQPSV	<p>Pink: Mg²⁺ binding Blue: SAM binding Yellow: Substrate binding</p> <p>Identity: 94/215 (43.7%) Similarity: 147/215 (68.4%)</p>
Danio Tomt	43	GISREERAFQYILTHATPGDSQSILDTFTWCSKVEFISNIGPKKGIKILDRLLQENCPIT	
		* :*: * :*: * :*: * :*: * :*: * :*: * :*: * :*: * :*: * :*: * :*: * :*: * :*	
		* :*: * :*: * :*: * :*: * :*: * :*: * :*: * :*: * :*: * :*: * :*: * :*	
Human S-COMT	62	LLELGAYCGYSAVRMARLLSPGARLITTEINPDCAAITQRMVDFAGVKDK-VTLVVGASQ	
Danio Tomt	103	VLELGTTCGYSYVNRMARSLPIGARISVEMDQRNAQVAEKIIRLAGFDDDMVELIQRPST	
		:****:****:**** * . ***: **: * :*: * :*: * :*: * :*: * :*: * :*: * :*	
		:****:****:**** * . ***: **: * :*: * :*: * :*: * :*: * :*: * :*: * :*	
Human S-COMT	121	DIIPQLKKKYDVTLDVFLDHWKDRVLPDTLLLECGLLRKGTVLLADHWICPGADPFL	
Danio Tomt	163	EVIPRLREDLGVRLDLVLMHWKRCYLPDLHLLEDGLIGQGSIIILADHWVIFPGAPNFL	
		:****: * . * :*: * :*: * :*: * :*: * :*: * :*: * :*: * :*: * :*: * :*	
		:****: * . * :*: * :*: * :*: * :*: * :*: * :*: * :*: * :*: * :*: * :*	
Human S-COMT	181	AHVRGSSCFECTHYQSFLY-REVVDGLEKAIYKGPSEAGP	
Danio Tomt	223	RYARRCGLYEVVRHRTLEYMRGIPDGMALTYIGIK-----	
		:* . . : * :*: * :*: * :*: * :*: * :*	
		:* . . : * :*: * :*: * :*: * :*: * :*	



428
429

430 **Figure 7.** Comta-GFP cannot restore basal MET channel activity in *mercury* mutant hair cells. **A** –
431 Alignment between the putative enzymatic domains of human S-COMT (amino acids 2-221,
432 Accession # NP_009294) and zebrafish Tomt (amino acids 43-259, Accession # ANO40802).
433 Residues involved in Mg²⁺-binding (pink), S-adenosylmethionine (SAM) binding (blue), and catechol
434 substrate binding (yellow) are indicated, as determined by the crystal structure for human S-COMT
435 (PDB_3BWM). Alignment legend - star (*) = conserved; colon (:)= conservative change; period (.) =
436 semi-conservative change. **B** – Representative images of Comta-GFP (left panels), FM 4-64 (middle
437 panels) and merged GFP and FM 4-64 channels (right panels) in lateral line NMs of *Tg(myo6b:comta-*
438 *GFP)* wild-type siblings and *tomt^{nl16}* mutants at 6 dpf. **C** – Quantification of FM 4-64 fluorescence
439 intensity per NM for 6 dpf *Tg(myo6b:comta-GFP)* siblings (*n* = 5 larvae, 8 NMs) and *tomt^{nl16}* mutants (*n*
440 = 3 larvae, 9 NMs). Error bars are the mean +/- SD. Asterisks indicate *p* < 0.0001 by unpaired, two-
441 tailed t-test. Scale bars = 5 μm in B, C.

442

443 **COMT methyltransferase active site residues are not required for Tomt activity**

444
445 The COMT enzyme catalyses the transfer of the methyl group from S-adenosylmethionine
446 (SAM/AdoMet) to the meta-hydroxyl group (3-O-methylation) of its catechol substrate (Axelrod and
447 Tomchick, 1958). The crystal structure for human COMT (structure PDB_3BWM) has revealed that
448 the cluster of amino acids Asp_{141/191}, His_{142/192}, Trp_{143/193}, and Lys_{144/194} are located in the
449 active site (human S-COMT / MB-COMT amino acid numbering, Figure 8A) (Rutherford et al., 2008;
450 Vidgren et al., 1994). Asp_{141/191} coordinates a requisite Mg²⁺ ion, His_{142/192} and Trp_{143/193}
451 interact with the SAM methyl donor, while Lys_{144/194} interacts with the catechol substrate and may
452 aid in catalysis. This DHWK motif is conserved in all vertebrate COMT orthologs and some vertebrate
453 Tomt proteins, most notably those from non-mammalian species. Interestingly, mammalian TOMT
454 proteins retain only the histidine in this region (armadillo / mouse H183 and human H216, Figure 8A).
455 The lack of conservation of these active site residues is surprising if Tomt shares the same substrates
456 as COMT. To see if a mammalian TOMT was functional in zebrafish, we expressed mouse TOMT-GFP
457 in *mercury* mutants (*Tg(myo6b:Mmu.Tomt-GFP)*). Using FM 4-64 label as an assay for MET channel
458 activity in lateral line hair cells, we find that Mmu.TOMT-GFP can significantly restore
459 mechanotransduction to *mercury* mutants ($p < 0.0001$; Figure 8B, C), albeit not to wild-type levels ($p <$
460 0.0001). This mild reduction in the efficacy of mouse TOMT to fully rescue FM label in *mercury*
461 mutant zebrafish could be due to differences in TOMT localization or protein sequence relative to the
462 endogenous zebrafish Tomt protein. However, as with the *Danio* Tomt-GFP transgene, homozygous
463 *mercury* mutants expressing Mmu.TOMT-GFP are viable, fertile, and do not exhibit obvious
464 behavioral phenotypes (data not shown).

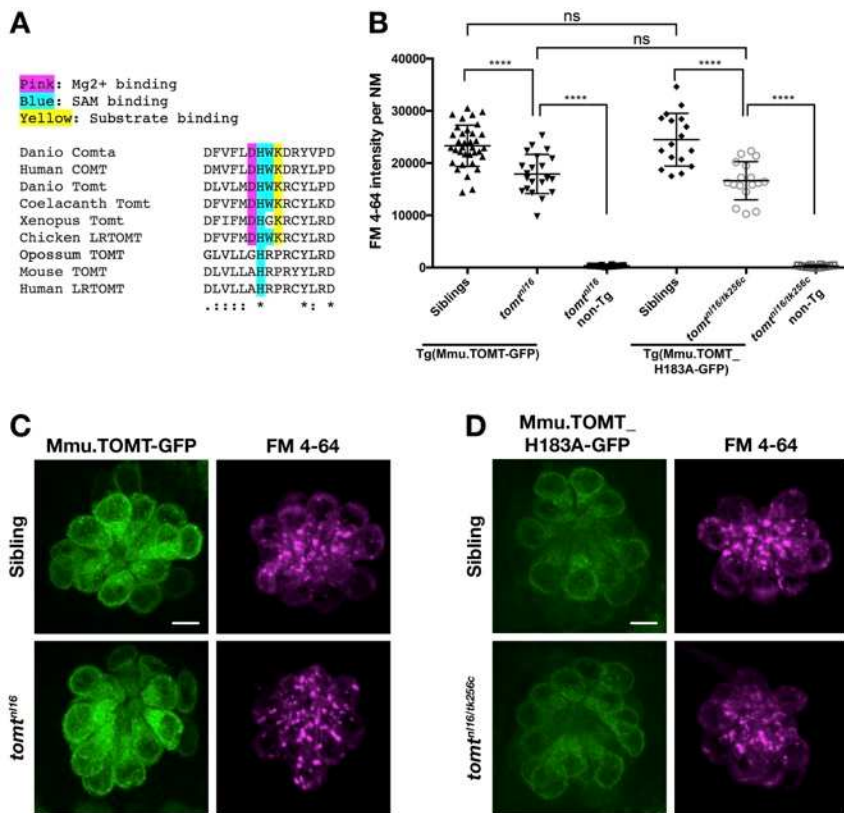


Figure 8. Mouse TOMT can restore basal MET channel activity to *mercury* mutant hair cells. **A** – Alignment between putative active site residues in *Danio rerio* Comta (Asp178-Asp192; NP_001025328), Human MB-COMT (Asp186-Asp200; NP_000745), and Tomt/LRTOMT proteins from *Danio rerio* (Asp178-Asp19; ANO40802), Coelacanth (Asp178-Asp192; XP_006003643), *Xenopus tropicalis* (Asp206-Asp220; XP_004920324), Chicken

479 (Asp178-Asp192; NP_001269010), Opossum (Gly177-Asp191; XP_016277512), Mouse (Asp177-Asp191;
 480 NP_001269017), and Human (Asp200-Asp214; NP_001138781). The shaded residues and alignment
 481 legend are the same as for Figure 7. **B** – Quantification of FM 4-64 fluorescence intensity per NM for
 482 *tomt* mutants stably expressing either mouse TOMT-GFP (*myo6b:Mmu.Tomt-GFP*; *n*=8, 22 NMs) or
 483 mouse TOMT-H183A-GFP (*myo6b:Mmu.Tomt_H183A-GFP*; *n*=7, 17 NMs). For comparison, FM 4-64
 484 fluorescence values are included for transgenic siblings (TOMT-GFP: *n*=12, 35 NMs; TOMT-H183A:
 485 *n*=8, 17 NMs) and non-transgenic mutants (*tomt*^{nl16}: *n*=4; 10 NMs; *tomt*^{nl16/tk256c}: *n*=6, 12 NMs). Error
 486 bars are the mean +/- SD. Asterisks indicate *p* < 0.0001 by one-way ANOVA with Bonferroni's
 487 multiple comparison test. **C** – Representative images of Mmu.TOMT-GFP (left) and FM 4-64 (right) in
 488 lateral line NMs of a 5 dpf *Tg(myo6b:Mmu.Tomt-GFP)* sibling (top) and a *tomt*^{nl16} mutant (bottom). **D**
 489 – Representative images of Mmu.TOMT_H183A-GFP (left) and FM 4-64 (right) in lateral line NMs of a
 490 4 dpf *Tg(myo6b:Mmu.Tomt_H183A-GFP)* sibling (top) and a *tomt*^{nl16/tk256c} mutant (bottom). Images in
 491 C and D were near the mean of the FM 4-64 values shown in B. Scale bars = 5 μm in C, D.
 492 The lack of amino acid sequence conservation between COMT and TOMT in the active site has been
 493 noted previously (Ehler et al., 2014). Although the native D182A substitution makes it unclear
 494 whether mammalian TOMT proteins can use Mg²⁺, it has been suggested that H183 may serve as the

495 catalytic residue due to the K185P substitution present in mammalian TOMT proteins (Ehler et al.,
496 2014). To test whether H183 was required for TOMT function, we established a stable transgenic line
497 of fish expressing *Mmu.Tomt_H183A-GFP* in hair cells. TOMT-H183A can significantly rescue FM 4-64
498 label in *mercury* mutants at levels indistinguishable from wild-type mouse TOMT ($p < 0.0001$; Figure
499 8B, D). And again, homozygous *mercury* mutants with the TOMT-H183A transgene are viable, fertile,
500 and do not exhibit obvious behavioral phenotypes. These results indicate that none of these COMT
501 active site residues are strictly required by TOMT to mediate mechanotransduction in hair cells.

502

503 **Localization of MET complex proteins Lhfpl5a, Pcdh15a, Tmie, Tmc 1 and Tmc2b in *mercury*** 504 **mutants**

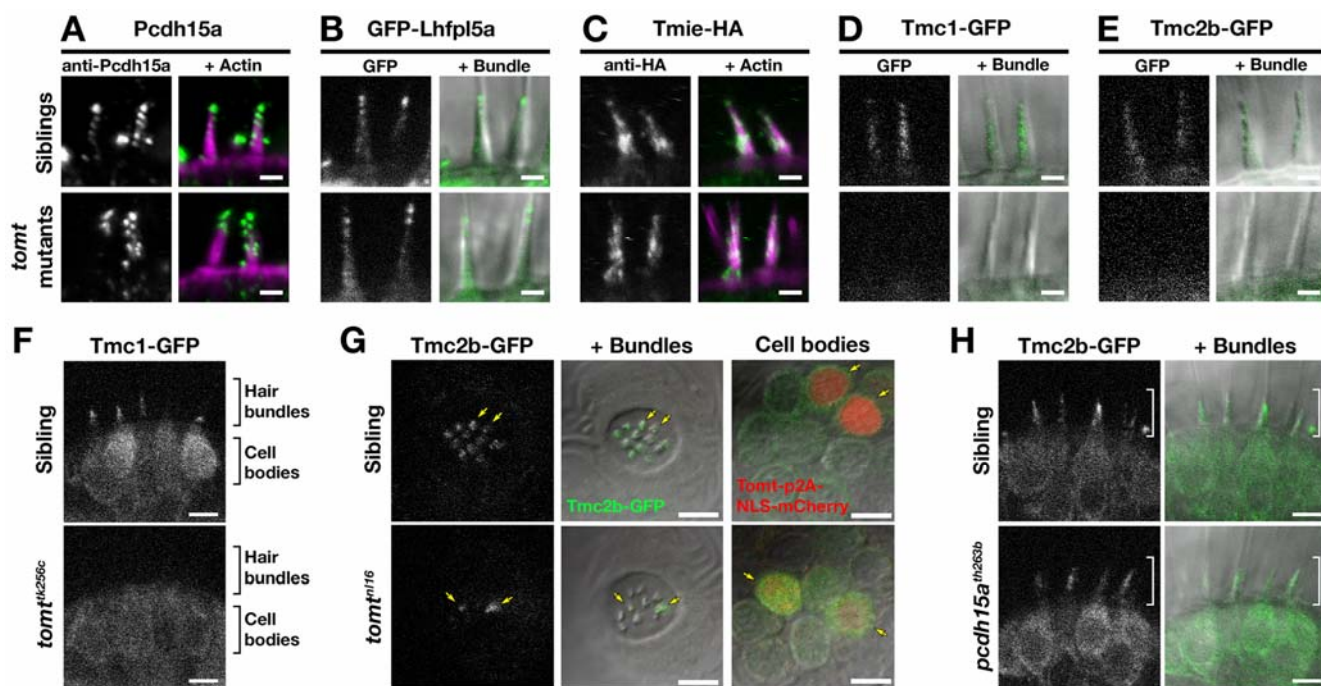
505

506 Two lines of evidence lead us to test whether *Tomt* regulates the trafficking and localization of MET
507 complex components. First, *Tomt* itself is enriched in the Golgi apparatus and excluded from the hair
508 bundle (Figure 2). Thus, it is well positioned within the secretory pathway to modulate protein
509 trafficking or function. Secondly, since COMT activity cannot rescue the *mercury* phenotype, the
510 mechanotransduction defect in *mercury* mutants is unlikely to be caused by a failure to metabolize
511 catecholamines (Figure 7). Thus, we examined whether the MET complex proteins Lipoma HMGIC
512 Fusion Partner-Like 5 (Lhfpl5a), Protocadherin 15a (Pcdh15a), Transmembrane Inner Ear (Tmie), and
513 Transmembrane channel-like (Tmc) are correctly localized to the hair bundle of inner ear hair cells in
514 *mercury* mutants (Figure 9A-E). For Pcdh15a, we used a previously characterized antibody that
515 recognizes an N-terminal epitope present in both the CD1 and CD3 isoforms (Maeda et al., 2017,
516 2014). To localize Lhfpl5a, Tmie, Tmc1 and Tmc2b, we used stably-integrated GFP or HA-tagged
517 transgenes that are functional and able to rescue their respective mutant phenotypes (Figure 9 -
518 supplement 1; data not shown). Pcdh15a, GFP-Lhfpl5a, and Tmie-HA can still be trafficked to the hair

519 bundle in *mercury* mutants (Figure 9A - C). However, neither Tmc1-GFP nor Tmc2b-GFP is detectable
520 in the hair bundle of Tomt-deficient hair cells (Figure 9D-E), although the GFP signal remains in the
521 cell body (Figure 9F – Tmc1-GFP; Tmc2b-GFP not shown). When overexpressed as transgenes, none
522 of these MET complex proteins can rescue basal MET channel activity in *mercury* mutants (Figure 9 –
523 supplement 2). Mosaic expression of a *tomt-P2A-NLS-mCherry* construct in *tomt^{nl16}* mutants can
524 rescue the bundle localization of Tmc2b-GFP (Figure 9G; *n* = 3 individuals, 12 cells), confirming that
525 Tomt is required cell autonomously for Tmc trafficking to the hair bundle.

526

527 To determine if the defect in Tmc localization was secondary to a loss of mechanotransduction in
528 Tomt-deficient hair cells, we imaged Tmc2b-GFP localization in *pcdh15a* (*orbiter; th263b*) mutants.
529 This null allele (R360X) of *pcdh15a* exhibits a similar phenotype to *mercury* mutants: no microphonics,
530 no acoustic startle response, and no FM dye label of lateral-line hair cells (Maeda et al., 2017;
531 Nicolson et al., 1998). Tmc2b-GFP was still able to localize to the hair bundle of *pcdh15a* mutants,
532 suggesting that Tmc protein localization is independent of Pcdh15a function and does not require
533 mechanotransduction (Figure 9H). Together these results suggest that Tomt is specifically required
534 for the correct trafficking of Tmc proteins to the hair bundle.



535

536 **Figure 9.** Hair bundle localization of MET complex proteins Lhfpl5a, Pcdh15a, Tmie, Tmc1 and Tmc2b
 537 in *mercury* mutants. **A-E** – Representative images of (A) anti-Pcdh15a (Sibs and *tomt*^{nl16} n = 4 each),
 538 (B) GFP-Lhfpl5a (Sibs and *tomt*^{tk256c} n = 12 each), (C) Tmie-HA (Sibs and *tomt*^{tk256c} n = 15 each), (D)
 539 Tmc1-GFP (Sibs n = 17; *tomt*^{tk256c} n = 10), and (E) Tmc2b (Sibs n = 16; *tomt*^{tk256c} n = 12) in lateral cristae
 540 hair bundles at 4-5 dpf. Images in B, D, and E are from live larvae, while those in A and C are from
 541 immunolabeled, fixed specimens with phalloidin-labeled actin shown in magenta. **F** – Optical
 542 sections through lateral cristae sensory patches showing the absence of Tmc1-GFP fluorescence
 543 specifically in the hair bundles of *tomt*^{tk256c} mutants, whereas GFP signal is present in the cells bodies.
 544 **G** – Tomt can restore Tmc2b-GFP localization to the hair bundle of *mercury* mutant hair cells. Tmc2b-
 545 GFP fluorescence in neuromast hair cells of a 4 dpf *Tg(myo6b:tmc2b-GFP)* wild-type sibling (top) and
 546 *tomt*^{nl16} mutant (bottom) transiently expressing *tomt-p2a-nls-mCherry*. Note the presence of Tmc2b-
 547 GFP only in the Tomt-P2A-nls-mCherry expressing cells of the *tomt*^{nl16} mutant (yellow arrows, n = 3
 548 individuals; 12 cells). **H** – Representative images of Tmc2b-GFP (left panels) and merged GFP and DIC
 549 channels (right panels) in the lateral cristae of 4 dpf siblings (n = 6; top) and *pcdh15a*^{th263b} mutants (n =
 550 6; bottom). White brackets indicated the hair bundle region of the hair cells. Scale bars = 2 μm in A-E,
 551 5 μm in F-H.

552

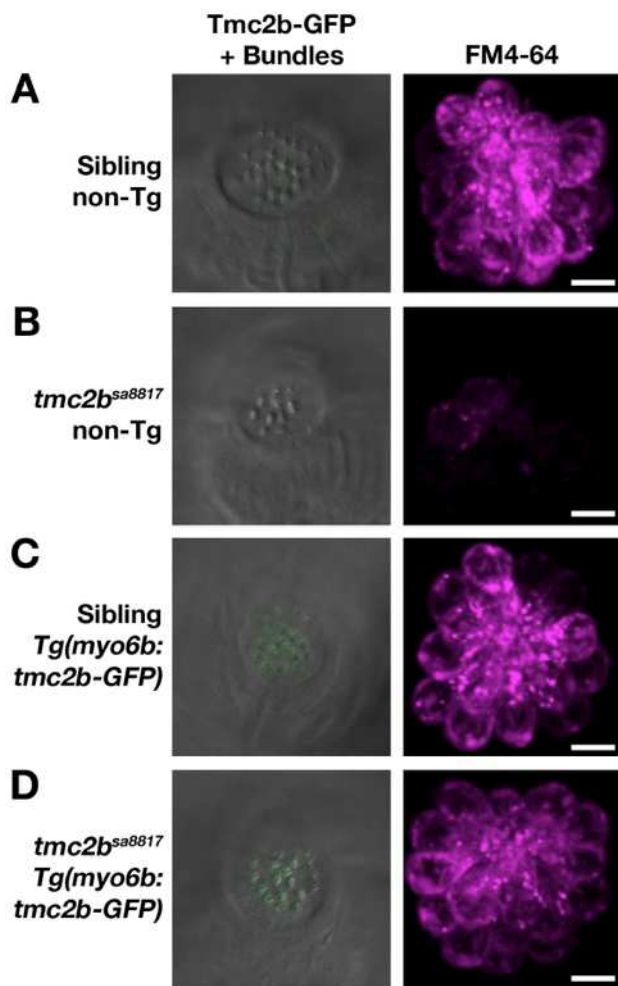
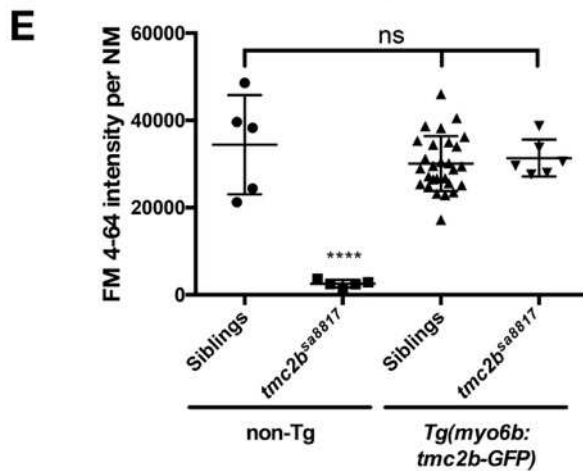
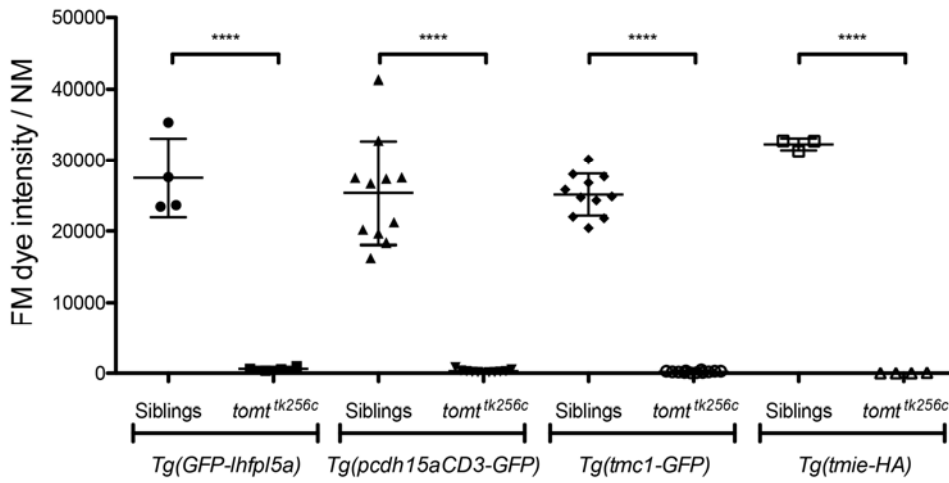


Figure 9 – figure supplement 1. Tmc2b-GFP can restore basal MET channel activity to *tmc2b^{sa8817}* mutants. **A-D** – Representative, merged GFP-DIC images of neuromast hair bundles (left) and FM 4-64 label (right) in 6 dpf non-transgenic, wild-type siblings (A), non-transgenic, *tmc2b^{sa8817}* mutants (B), *Tg(myo6b:tmc2b-GFP)*, wild-type siblings (C), and *Tg(myo6b:tmc2b-GFP)*, *tmc2b^{sa8817}* mutants (D). **E** – Quantification of FM 4-64 fluorescence intensity per NM for the genotypes shown in A-D. Non-transgenic siblings: *n* = 3 larvae, 5 NM. Non-transgenic *tmc2b^{sa8817}*: *n* = 3 larvae, 5 NM. *Tg(tmc2b-GFP)* siblings: *n* = 10 larvae, 28 NM. *Tg(tmc2b-GFP) / tmc2b^{sa8817}*: *n* = 2 larvae, 6 NM. Error bars are the mean +/- SD. ns = not significant. Asterisks indicate *p* < 0.0001 by one-way ANOVA with Bonferroni's multiple comparison test. Scale bars = 5 μ m in A-D.





572

573 **Figure 9 – figure supplement 2.** Transgenic expression of GFP-Lhfp15a, Pcdh15aCD3-GFP, Tmc1-
 574 GFP, or Tmie-HA cannot restore basal MET channel activity to *mercury* mutant hair cells.

575 *Tg(myo6b:GFP-lhfp15a)* 4 dpf: siblings $n = 2$ larvae, 4 NM; *tomt^{tk256c}* $n = 2$ larvae, 4 NM.

576 *Tg(myo6b:pcdh15aCD3-GFP)* 5 dpf: siblings $n = 5$ larvae, 11 NM; *tomt^{tk256c}* $n = 4$ larvae, 11 NM.

577 *Tg(myo6b:tmc1-GFP)* 5 dpf: siblings $n = 4$ larvae, 11 NM; *tomt^{tk256c}* $n = 4$ larvae, 12 NM. *Tg(myo6b:tmie-*

578 *HA)* 5 dpf: siblings $n = 2$ larvae, 3 NM; *tomt^{tk256c}* $n = 2$ larvae, 4 NM. Error bars are the mean +/- SD.

579 Asterisks indicate $p < 0.0001$ by unpaired, two-tailed t-tests.

580

581

582 **Mouse TMC1 can directly interact with wild-type TOMT and TOMT-H183A**

583

584 The observation that Tomt is required for Tmc trafficking to the hair bundle suggested that these
585 proteins might interact. We tested idea this by co-expressing mouse TOMT and TMC1 in HEK 293
586 cells and performing co-immunoprecipitation experiments. TMC1-GFP was co-expressed with HA-
587 tagged TOMT or TOMT-H183A, as well as the HA-tagged controls COMT, EZRIN (EZR), or RI α
588 subunit of protein kinase A (PRKAR1A) (Figure 10A, B). HA immunoprecipitates were blotted for the
589 presence of TMC1 (Figure 10C, D). TOMT and TMC1 can directly interact, and this interaction is
590 reproducibly enhanced by the H183A change in TOMT (Figure 10D). There was no detectable
591 interaction between TMC1 and COMT, EZR, or PRKAR1A. Likewise, the same pattern of interactions
592 was detected when lysates were immunoprecipitated with anti-GFP and blotted for HA (Figure 10E,
593 F). However, this interaction did not alter the subcellular localization of TMC1-GFP in HEK 293 cells;
594 both TOMT and TMC1 were associated with intracellular membranes (Figure 10 – figure supplement
595 1). These co-immunoprecipitation results suggest that TOMT and TMC1 can directly interact, and
596 support a model where TOMT interacts with the TMCs in the secretory pathway of hair cells to
597 mediate TMC trafficking to the hair bundle.

598

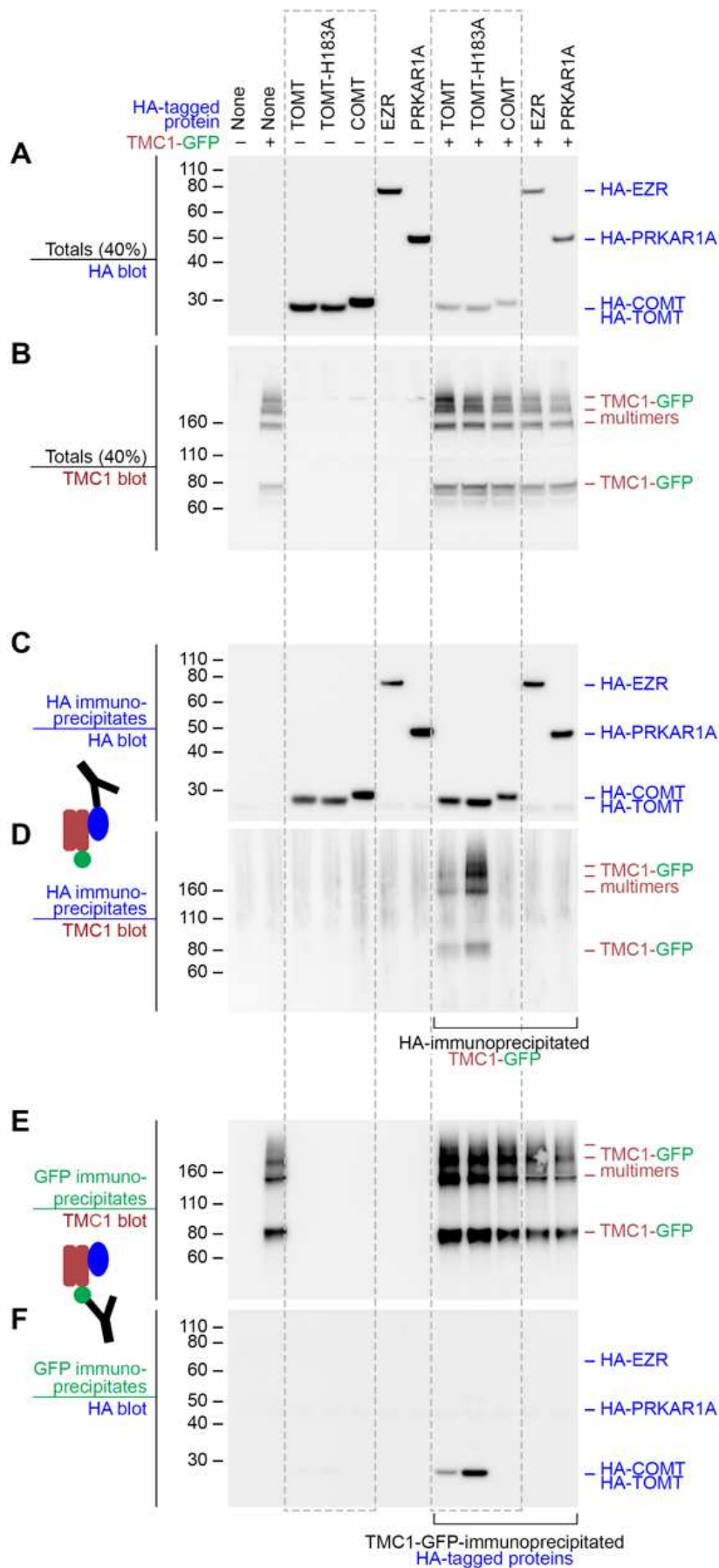


Figure 10. Mouse TOMT and TMC1 can interact in HEK 293 cells. Top labels: transfected proteins for all blots. Blue labels: HA-tagged proteins; Burgundy: TMC1; Green: GFP. **A** – Anti-HA blot of totals (40% loaded relative to immunoprecipitates). **B** – Anti-TMC1 blot of totals. **C** – Anti-HA blot of HA immunoprecipitates. **D** – TMC1 blot of HA immunoprecipitates. **E** – TMC1 blot of GFP immunoprecipitates (immunoprecipitating GFP-TMC1). **F** – HA blot of GFP immunoprecipitates. In both HA and GFP immunoprecipitation experiments, a robust interaction was detected between TOMT and TMC1; the H183A change in TOMT enhances this interaction. The HA-tagged controls COMT, EZR, and PRKAR1A did not interact with TMC1-GFP.

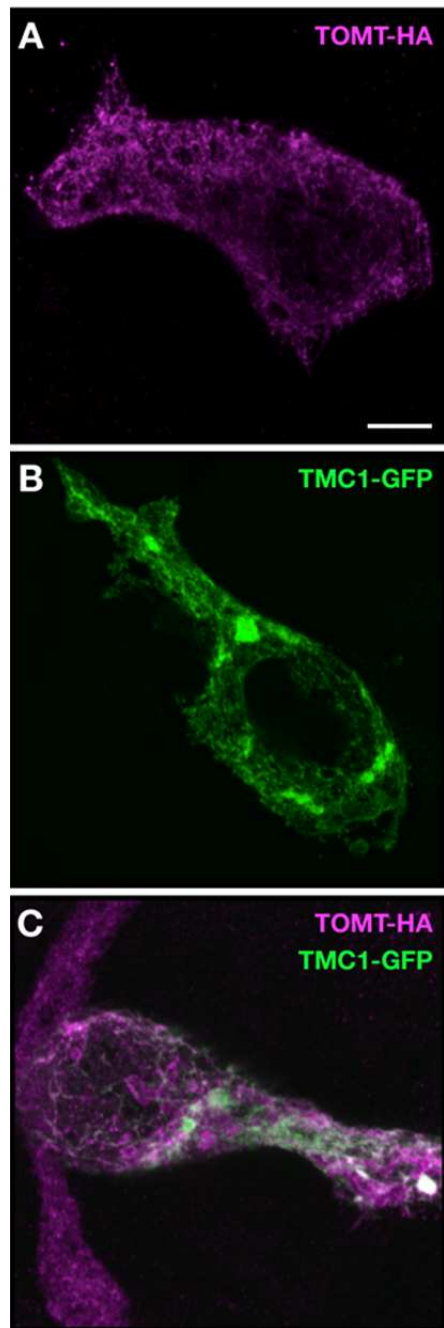


Figure 10 – figure supplement 1. TOMT-HA and TMC1-GFP in HEK 293 cells. **A** – TOMT-HA only; **B** – TMC1-GFP only; **C** – TOMT-HA (magenta) and TMC1-GFP (green) co-expressed. Both TOMT and TMC1 were confined to intracellular membranes. Scale bar = 5 μm , applies to A-C.

631 **Discussion**

632
633 In this study we report that mutations in *transmembrane O-methyltransferase (tomt)* are responsible
634 for the *mercury* mutant found in a screen for hearing and balance genes in zebrafish (Nicolson et al.,
635 1998). *tomt* is the zebrafish ortholog of the human *LRTOMT2* gene, mutations in which are
636 responsible for non-syndromic deafness DFNB63 (Ahmed et al., 2008; Du et al., 2008). Studies using
637 the mouse model of DFNB63 suggested that TOMT functions as a catechol O-methyltransferase, and
638 that the failure of hair cells to metabolize catecholamines leads to a degenerative phenotype and
639 subsequent hearing loss (Du et al., 2008). However, progressive degeneration of hair cells is a
640 common phenotype amongst mechanotransduction mutants in mice (Alagramam et al., 2000;
641 Kawashima et al., 2011; Longo-Guess et al., 2005; Mitchem et al., 2002; Steel and Bock, 1980). It was
642 not clear if aberrant catecholamine metabolism was truly responsible for the observed hair cell
643 degeneration, nor whether *Tomt*-deficient hair cells had mechanotransduction defects prior to
644 degenerating.

645

646 To clarify the role of *Tomt* in hair cell function, we used the zebrafish *mercury* mutant as a model for
647 DFNB63. In the present study we show that *Tomt*-deficient hair cells have a specific defect in
648 mechanotransduction. *Tomt*-deficient hair cells have no evoked MET current and do not label with
649 MET channel permeant FM dyes (Figures 4 and 5). The behavioral and physiological phenotypes can
650 both be rescued by expression of *Tomt*-GFP specifically in hair cells (Figures 3 and 5). We determined
651 that the absence of mechanotransduction was not due to a general developmental defect by using a
652 heat shock approach to express *Tomt*-GFP in mature hair cells. Heat shock-inducible *Tomt*-GFP was
653 able to restore MET channel function to mature mutant hair cells, indicating that *Tomt*-deficient hair
654 cells are otherwise competent for mechanotransduction, but actively require *Tomt* function (Figure

655 6). Based on these results, we propose that a defect in hair cell mechanotransduction is the cause of
656 hearing loss in *tomt* mutants and DFNB63 patients.

657

658 Our data suggest that the absence of mechanotransduction in *tomt* mutants is caused by defects in
659 Tmc protein trafficking. Using GFP-tagged versions of zebrafish *Tmc1* and *Tmc2b*, we show that Tmc
660 proteins do not correctly localize to the hair bundle of *Tomt*-deficient hair cells (Figure 9). This
661 trafficking defect can be rescued by transgenic expression of *Tomt*. Like *Tomt*-deficient hair cells,
662 TMC1/2 double knockout hair cells do not label with FM, have no evoked mechanotransduction
663 currents, but have normal voltage-dependent currents (Kawashima et al., 2011). Likewise, *mercury*
664 hair cells exhibit only mild defects in bundle morphology (Figure 5 – figure supplement 1). This
665 phenotype is similar to that observed in *Tmc1/2* double knockout mice at early stages when TMC-
666 deficient hair cells have no mechanotransduction current, but still have tip links and relatively normal
667 bundle morphology. Furthermore, the time course of hair cell degeneration in TOMT-deficient mice
668 is very similar to that observed for TMC-null mice (Du et al., 2008; Kawashima et al., 2011). Given the
669 similarities between *Tomt* and *Tmc* mutant mice, it is likely that the zebrafish *mercury* mutant is
670 equivalent to a triple *tmc1/2a/2b* knockout.

671

672 Typically, proteins that are involved in mechanotransduction are themselves localized in the hair
673 bundle, the mechanosensitive organelle of the hair cell. However, neither *Tomt*-GFP, *Tomt*-HA,
674 *Tomt*(1-45)-GFP nor *Mmu.TOMT* are detectable in the hair bundle. Rather, these proteins are
675 localized to the secretory pathway, with the zebrafish proteins showing enriched localization in the
676 Golgi apparatus (Figures 2 and 8). This intracellular location suggests that *Tomt* is regulating Tmc
677 protein localization prior to the point at which the Tmcs are trafficked to the hair bundle. Although

678 zebrafish Tomt is enriched in the Golgi compartment, this enrichment does not appear to be
679 necessary for function. When transgenically expressed in zebrafish hair cells, Mmu.TOMT-GFP
680 appears to be primarily located in the ER, yet can still restore MET channel activity to *mercury*
681 mutants (Figure 8). We cannot exclude the possibility that Mmu.TOMT is also present in the Golgi
682 apparatus, but enrichment within that organelle is not strictly required for function. Since other
683 known members of the MET channel complex can localize to the bundle in *mercury* mutants (Figure
684 9), we propose that Tomt is actively required for the trafficking of Tmc proteins to the hair bundle
685 where the Tmcs can then form a functional MET complex with Pcdh15, Lhfpl5, and Tmie. As such,
686 LRTOMT / TOMT may be a suitable target for gene therapy, as has been shown for the TMCs (Askew
687 et al., 2015). These data suggest that Tomt regulates Tmc protein trafficking (and therefore
688 mechanotransduction) from within the secretory pathway, and does not directly participate in the
689 MET complex.

690

691 The mechanisms by which Tomt regulates Tmc protein trafficking in hair cells are still not clear.
692 However, we suggest that the mechanotransduction defects are not caused by a failure of hair cells
693 to metabolize catecholamines. We find that Comta, a closely related O-methyltransferase, cannot
694 restore mechanotransduction to *mercury* mutants (Figure 7). This result argues against the idea that
695 Tomt is primarily responsible for catecholamine metabolism in hair cells. Additionally, transcriptomic
696 and proteomic surveys of mouse and chick hair cells shows that *Comt* is endogenously expressed in
697 hair cells and the surrounding cell types (Scheffer et al., 2015; Shen et al., 2015; Shin et al., 2013), yet
698 is unable to compensate for the loss of TOMT. Furthermore, we show that COMT active site residues
699 are not absolutely required for TOMT activity in hair cells (Figure 8), suggesting that TOMT and
700 COMT proteins perform unique functions.

701

702 COMT can methylate a variety of catechol-containing substrates, with methylation of the 3'-hydroxyl
703 (meta) favored over the 4'-hydroxyl (para) by about 5:1 *in vitro* (Zhang and Klinman, 2011). While an
704 exhaustive survey has not been done, single amino acid substitutions in COMT can decrease its
705 affinity for catechol substrates, decrease the meta:para ratio, and change the rate of catalysis (Law
706 et al., 2016; Zhang et al., 2015; Zhang and Klinman, 2011). Although human COMT and Danio Tomt
707 are 44% identical and 68% similar within their putative enzymatic domains (Figure 7), those residues
708 where they differ may have important consequences for Tomt methyltransferase activity towards
709 catechols.

710

711 Using the COMT crystal structure as a guide, we find that there are some potentially important
712 differences between the two enzymes, especially comparing mammalian COMT and TOMT. In S-
713 COMT, the amino acid residues Asp141, Asp169, and Asn170 coordinate a Mg²⁺ ion that is required to
714 correctly orientate the hydroxyl groups of the catechol in the active site for methylation (Vidgren et
715 al., 1994). Of these three residues, only TOMT Asp210 (orthologous to S-COMT Asp169) is
716 conserved, suggesting that TOMT may not require a divalent ion in order to function. Mammalian
717 TOMT proteins also differ from COMT with respect to other active site residues, most notably the
718 putative catalytic residue Lys144 in S-COMT. Depending on the substrate, mutating COMT Lys144 to
719 an alanine dramatically reduces or abolishes the methyltransfer reaction, and can change the
720 meta:para ratio (Law et al., 2016). It has been suggested that His183 could take over as the catalytic
721 residue in TOMT due to the native Lys185Pro substitution (Ehler et al., 2014). However, the mouse
722 TOMT-H183A-GFP protein can still rescue the mechanotransduction and behavioral defects in
723 *mercury* mutants (Figure 8). Interestingly, the His183Ala change also enhances the biochemical

724 interaction between TOMT and TMC₁ in cultured cells (Figure 10). Together with the possibility that
725 TOMT does not bind divalent cations, these results call into question whether TOMT functions as a
726 catechol O-methyltransferase *in vivo*. Consistent with this idea is the finding that TOMT exhibited
727 only modest catechol O-methyltransferase activity *in vitro*, even when supplied with
728 supraphysiological levels of norepinephrine (Du et al., 2008). Thus, Tomt's *bona fide* physiological
729 target has yet to be identified.

730

731 Given the evidence that TOMT is unlikely to be a functional catechol O-methyltransferase *in vivo*, the
732 question now becomes: what is TOMT doing to regulate TMC protein trafficking in hair cells? Is it a
733 methyltransferase and what is its substrate? Or is it performing a non-enzymatic function? There are
734 precedents for methylation events regulating protein function and trafficking. Intriguingly, another
735 COMT-related protein, Catechol O-methyltransferase domain containing protein 1 (COMTD1 /
736 MT773), has been shown to stimulate epithelial Na⁺ channel (ENaC) currents (Edinger et al., 2006).
737 Protein O-methylation is also involved in Ras protein trafficking (Clarke, 1992) and the function of a
738 bacterial chemotaxis sensory system (Falke et al., 1997). However, the idea that TOMT is a protein
739 methyltransferase is speculative at this point. Alternatively, the role of TOMT in sensory hair cells
740 may be independent of an enzymatic function, as has been shown for some methyltransferases in
741 other systems (DebRoy et al., 2013; Dong et al., 2008; Perreault et al., 2009). The protein-protein
742 interaction between TOMT and TMC₁ presents the possibility that TOMT acts as a chaperone to
743 facilitate TMC protein folding or trafficking. However, we did not observe a redistribution of TMC₁-
744 GFP localization to the plasma membrane of HEK 293 cells when co-expressed with TOMT (Figure 10
745 – figure supplement 1). This suggests that other factors in hair cells are involved in modulating TMC
746 localization. More work is required to determine if TOMT is a methyltransferase *in vivo*, to identify its

747 substrate, and to understand the functional consequences of the interaction between TOMT and the
748 TMCs in sensory hair cells.

749

750 **Materials and Methods**

751

752 ***Ethics Statement***

753 Zebrafish (*Danio rerio*) were maintained at 28°C and bred using standard conditions. Animal research
754 complied with guidelines stipulated by the Institutional Animal Care and Use Committed at Oregon
755 Health and Science University. Electrophysiological recordings from zebrafish larvae were licensed
756 by the Home Office under the Animals (Scientific Procedures) Act 1986 and were approved by the
757 University of Sheffield Ethical Review Committee. The following zebrafish mutant alleles were used
758 for this study: *pcdh15a*^{th263b}, *tomt*^{nl16}, and *tomt*^{tk256c} (Nicolson et al., 1998; Seiler et al., 2005). The
759 *tmc2b*^{sa8817} allele was obtained from the Wellcome Trust Sanger Institute Zebrafish Mutation Project
760 (Kettleborough et al., 2013). All lines were maintained in a Tübingen or Tüpfel long fin wild-type
761 background. For all experiments, we used larvae at 2-6 dpf, which are of indeterminate sex at this
762 stage.

763

764 ***Genotyping***

765 Adult fish were genotyped by fin clipping; see Supplemental File 1A for *pcdh15a*^{th263b}, *tomt*^{nl16/tk265c}
766 and *tmc2b*^{sa8817} genotyping primers. Mutant larvae were identified by either behaviour (auditory or
767 vestibular defects) and/or lack of FM dye label of neuromasts. For those experiments where
768 expression of a transgene rescued behaviour or FM dye label (Figures 3, 5, and 8), homozygous
769 mutant larvae were identified by single larvae DNA extraction (Meeker et al., 2007), followed by PCR
770 and sequencing.

771

772 ***RT-PCR, Gateway cloning and Tol2 Gateway transgenesis***

773 All primer sequences and expression constructs used in this study are provided in Supplemental File
774 1. RT-PCR for *tomt* and *lrrc51* was done by one-step RT-PCR (SuperScript III One-Step RT-PCR kit,
775 Thermo Fisher Scientific, Waltham, MA) using 840 ng of total RNA from 5 dpf *tomt*^{nl16} and *tomt*^{tk256c}
776 siblings and mutants following standard protocols. Gateway entry vector inserts were also cloned by
777 one-step RT-PCR using gene specific primers with integrated Gateway recombination sites. Total
778 RNA from 4-5 dpf larvae was used as the template for zebrafish genes, while mouse *Tomt* was cloned
779 from WT mouse utricle total RNA. Gateway entry vectors were made by standard techniques (Kwan
780 et al., 2007). The full-length open reading frames (ORF) of *tmc1* and *tmc2b* were obtained by 5'-RACE
781 or 3'-RACE by using total RNA extracted from whole larvae (SMARTer RACE cDNA Amplification Kit,
782 Takara Bio, Mountain View, CA). *tmc1* and *tmc2b* ORFs were subcloned into the pDONR221 middle
783 entry vector together with sequence coding for a peptide linker (GGGGS)₄ and a C-terminal
784 monomeric EGFP tag. Construction of final Gateway expression vectors (Supplemental File 1B) and
785 the generation of transgenic fish lines (Supplemental File 1C) were performed as previously described
786 (Kwan et al., 2007). pcDNA3.1(+)*Tomt*-HA and pcDNA3.1(+)*Comt*-HA were made by standard
787 cloning techniques using templates with *NheI* and *XhoI* sites added to the 5' end 3' ends by PCR.
788 pcDNA3.1(+)*Tomt*-H183A-HA and pDONR221-*Mmu.Tomt_H183A* were made using the Quikchange
789 Lightning site-directed mutagenesis kit (Agilent, Santa Clara, CA) according to the manufacturer's
790 protocol.

791

792 ***Acoustically evoked behavior response (AEBR)***

793 Quantification of the larval AEBR was performed using the Zebrabox monitoring system (ViewPoint
794 Life Sciences, Montreal, Canada) as previously described (Einhorn et al., 2012; Maeda et al., 2017).
795 Each group of six fish was subjected to two or three trials of 12 stimuli and, for each individual larva
796 the trial with best AEBR performance was used for quantification. Positive responses where
797 spontaneous movement occurred in the second prior to the stimulus were excluded from analysis.
798 Trials where spontaneous movement occurred for more than six of the twelve stimuli were also
799 excluded from analysis.

800

801 ***Electrophysiological recordings***

802 For *in vivo* hair cell recordings, larvae (3.0-5.2 dpf) were briefly treated with MS-222 before being
803 paralyzed by injecting 125 μ M α -bungarotoxin (Tocris, UK) into the heart (Olt et al., 2014). Whole-cell
804 patch clamp experiments were performed at room temperature (21–24°C) from hair cells of the
805 zebrafish primary neuromasts. Patch pipettes were made from soda glass capillaries (Harvard
806 Apparatus Ltd, Edenbridge, UK) and had a typical resistance in the extracellular solution of 3–5 M Ω .
807 In order to reduce the fast electrode capacitive transient, the shank of each capillary was coated
808 with surfboard wax. Basolateral membrane current recordings were performed using the following
809 intracellular solution: 131 mM KCl, 3 mM MgCl₂, 1 mM EGTA-KOH, 5 mM Na₂ATP, 5 mM Hepes-
810 KOH, and 10 mM sodium phosphocreatine (pH 7.3). For mechanoelectrical transduction, the patch
811 pipette was filled with an intracellular solution containing (in mM): 106 L-glutamic acid, 20 CsCl, 10
812 Na₂phosphocreatine, 3 MgCl₂, 1 EGTA-CsOH, 5 Na₂ATP, 5 HEPES and 0.3 GTP (the pH was adjusted
813 to 7.3 with CsOH, 294 mOsmol/kg). Recordings were made with an Optopatch (Cairn Research Ltd,
814 UK) or Multiplamp 900B (Molecular Devices, USA) amplifier. Data acquisition was performed using
815 pClamp software with a Digidata 1440A data acquisition board (Molecular Devices, USA). Recordings

816 were sampled at 5 kHz, low pass filtered at 2.5 kHz (8-pole Bessel) and stored on computer for offline
817 analysis (Origin and PClamp). Membrane potentials in voltage clamp were corrected for the liquid
818 junction potential, measured between electrode and bath solutions, of either -4 mV (KCl-based
819 intracellular) or -11 mV (L-glutamic acid-based intracellular). MET currents were elicited using a fluid
820 jet from a pipette driven by a 25 mm diameter piezoelectric disc (Corns et al., 2016, 2014; Kros et al.,
821 1992). The fluid jet pipette tip had a diameter of 12-16 μm and was positioned at about 8-14 μm from
822 the hair bundles in the neuromast. The distance of the pipette tip from the bundle was adjusted to
823 elicit a maximal MET current. Mechanical stimuli were applied as steps or 50 Hz sinusoids (filtered at
824 1 kHz, 8-pole Bessel). Mean values are quoted in text and figures as means \pm S.E.M.

825

826 ***Immunostaining and whole mount mRNA in situ hybridization***

827 Larvae were anesthetized with E3 plus 0.03% MS-222 and fixed in 4 % paraformaldehyde / 1x
828 Phosphate Buffered Saline (PBS) for 4 h at room temperature or overnight at 4°C followed by 5 \times 5
829 min washes in PBS/0.1 % Tween-20 (PBST). Fixed specimens were permeabilized with 0.5% triton-X
830 in PBS (3 x 20 minutes), and blocked > 2 hours in PBS / 1% bovine serum albumin / 1% DMSO / 5%
831 goat serum. Use of the anti-Pcdh15a antibody has been previously described (Maeda et al., 2017). To
832 label HA-tagged Tomt or Tmie, larvae were incubated in a 1:1000 dilution of rat anti-HA clone 3F10
833 antibody (Sigma-Aldrich, St. Louis, MO) in block overnight at 4 °C, washed 5 \times 15 min in 1x PBS/0.01
834 % Tween-20, incubated in a 1:1000 dilution of Dylight 549 goat anti-rat IgG (Jackson
835 ImmunoResearch, West Grove, PA) with 1:1000 dilution of Alexa Fluor 488 phalloidin (Thermo Fisher
836 Scientific), and washed again 5 \times 15 min in PBS/0.01 % Tween-20.

837

838 HEK 293 cells were plated in a 6-well cell culture dish and transfected using Effectene (Qiagen,
839 Germantown, MD) following the manufacturer's protocol. Each well received either no plasmid, 0.4
840 µg of TMC1-GFP, or 0.4 µg TMC1-GFP and 0.4 µg TOMT-HA. After 20 hours, cells were rinsed briefly
841 with PBS and fixed for 30 minutes in 4% formaldehyde at room temperature. Cells were rinsed 2x
842 with PBS, then permeabilized and blocked for 1 hour in 0.2% saponin and 5% normal donkey serum.
843 Cells were then incubated overnight with 1:500 anti-HA antibody (Proteintech, Rosemont, IL) diluted
844 in blocking solution (5% normal donkey serum in PBS). Cells were rinsed 3x with PBS for 5-10 minutes
845 each rinse and incubated for 3-4 hours with 1:1000 donkey anti-rabbit Alexa Fluor 568 secondary
846 antibodies (Thermo Fisher Scientific) and 1:500 Alexa Fluor 647 phalloidin (Thermo Fisher Scientific).
847 Cells were incubated with 1:5000 DAPI (Thermo Fisher Scientific) diluted in PBS for 10 minutes and
848 the rinsed 3x with PBS for 5-10 minutes each rinse. Coverslips were then mounted on slides with
849 Everbrite media (Biotium, Fremont, CA). Images were acquired using a 100X 1.46 NA Plan-
850 Apochromat objective on a Zeiss LSM780 with Airyscan processing.

851

852 Whole mount mRNA *in situ* hybridization (ISH) and probe synthesis was performed essentially as
853 described (Erickson et al., 2010; Thisse and Thisse, 2008). *tomt* antisense RNA probe synthesis was
854 done using NotI linearized pCR4 plasmid containing the full length *tomt* coding sequence as a
855 template. Specimens were mounted on a depression slide in 1.2 % low-melting point agarose and
856 imaged on a Leica DMLB microscope fitted with a Zeiss AxioCam MRc 5 camera using Zeiss
857 AxioVision acquisition software (Version 4.5).

858

859 ***FM dye labelling of hair cells***

860 To label neuromast hair cells, groups of four larvae were incubated in a 3 μ m solution of either FM 1-
861 43 or FM 4-64 (Thermo Fisher Scientific) in E3 embryo media for 30 seconds, followed by three rinses
862 in E3. To label hair cells of the inner ear, larvae were anesthetized with E3 plus 0.03% MS-222 and
863 mounted laterally on a depression slide in 1.2% low-melting point agarose / E3. Approximately 2 nl of
864 a 3 μ m FM1-43 solution was injected directly into the otic capsule, and the larvae were immediately
865 imaged. Because it is not possible to rinse out the FM dye from the otic capsule, some background
866 staining of hair bundles is observed in *mercury* mutants.

867

868 ***Imaging and quantification of fluorescence intensity***

869 For imaging, live larvae were anesthetized with E3 plus 0.03% MS-222 and mounted laterally on a
870 depression slide in 1.2% low-melting point agarose / E3 and imaged on a Zeiss LSM700 laser-
871 scanning confocal microscope with a Plan Aplanachromat 40x/1.0 water lens and Zeiss Zen software. To
872 quantify FM dye or GFP fluorescence intensity, unadjusted maximum projections were analyzed in
873 Image J (v. 1.48). Fluorescence intensity is reported as the background-subtracted Integrated
874 Density value. Figures were assembled and adjusted for brightness and contrast in Adobe Photoshop
875 (CS6). Where relevant, individual channels were adjusted equally for siblings and mutants, and
876 images chosen for Figures were near the mean of the group data. Because transient transgenesis can
877 cause variation in expression levels between individual cells, the mCherry channel only in Figure 9G
878 was differentially adjusted for brightness between the sibling and mutant images.

879

880 ***Statistical analysis and replicates***

881 For the purpose of this study, biological replicates are defined as the individual larvae analysed in
882 each experiment, the numbers of which are provided in the Figure legends. Data for quantification

883 and statistical comparisons are taken from single experiments, though at least two technical
884 replicates was performed for each experiment to confirm the results. All graphs and statistical
885 comparisons were done using GraphPad Prism v.6.0h.

886

887 ***Immunoprecipitation and immunoblotting***

888 HEK 293 cells were seeded in multiwell plates with 10-cm wells at 1×10^6 /dish. After 24 hours in
889 culture, they were transfected with the indicated DNA combination using Effectene (Qiagen). To
890 equalize protein expression, DNA was titrated to: 2 μg /dish TMC1-GFP, 0.25 μg /dish TOMT-HA, 0.5
891 μg /dish TOMT-H183A-HA, 0.1 μg /dish COMT-HA, 1 μg /dish HA-EZR, and 2 μg /dish HA-PRKAR1A.
892 Total DNA was adjusted to 4 μg /dish using empty pcDNA3. After 48 hours, the medium was
893 aspirated and the cells frozen rapidly at -80°C . Cell extracts were prepared using two 1-ml aliquots of
894 RIPA buffer (50 mM Tris pH 8.0, 150 mM NaCl, 0.1% SDS, 1% NP-40, 0.5% deoxycholate)
895 supplemented with protease inhibitors (Sigma-Aldrich, P8340). Insoluble material was removed by
896 centrifuging at $90,700 \times g$ (r_{av}).

897

898 Totals were prepared from 100 μl of extract with 100 μl 2X SDS-PAGE sample buffer (prepared from
899 LifeTech LDS sample buffer together with DTT). Immunoprecipitations from 250 μl extract were
900 accomplished with either 10 μl of 50 mg/ml Dynabeads MyOne Tosylactivated (#65502, Thermo
901 Fisher Scientific) coupled with 2 mg/ml recombinantly produced anti-GFP (gift of Hongyu Zhao) for 1
902 hr at room-temperature, or 10 μl of anti-HA-agarose (clone HA-7; Sigma-Aldrich, #A2095) overnight
903 at 4°C . Following incubation, beads were washed three times with RIPA buffer, and heated at 95°C
904 for 10 mins with two aliquots (90 μl) of 1X SDS-PAGE sample buffer (without DTT). After separation

905 from the adsorbent, eluates were adjusted to 50 mM DTT. Totals were thus 40% of
906 immunoprecipitates.
907
908 Samples were analyzed by SDS-PAGE using 4-12% gels with either MOPS (TMC1 immunoblots), or
909 MES (HA immunoblots) running buffer (Thermo Fisher Scientific). Proteins were transferred to 0.45
910 μm PVDF membrane (Millipore, Billerica, MA), stained with India Ink, blocked with ECL PRIME
911 blocking agent (GE Healthcare, Chicago, IL), and probed with rabbit anti-mmTMC1 (Maeda et al.,
912 2014) or anti-HA (clone HA-7; Sigma-Aldrich) antibodies. Protein bands were visualized with HRP-
913 coupled anti-rabbit or light-chain-specific anti-mouse (Jackson ImmunoResearch) and ECL PRIME
914 (GE Healthcare) using a FujiFilm LAS3000 imaging system.

915

916 **Acknowledgments**

917 This work was supported by the NIH (R01DC013572 and R01DC013531 to T.N., R01HD072844 to AN,
918 R01DC002368 and P30DC005983 to PGBG), the Max Planck Society (T.N.) and a Wellcome Trust
919 grant 102892 (W.M). Thank you to Leah Snyder, Daniel Gibson and Lisa Hayashi for fish care, and to
920 Matthew Avenarius (Barr-Gillespie lab) for mouse utricle RNA.

921 **Competing interests**

922 The authors declare that no competing interests exist.

923 **References**

- 924 Ahmed, Z.M., Masmoudi, S., Kalay, E., Belyantseva, I.A., Mosrati, M.A., Collin, R.W.J., Riazuddin, S.,
925 Hmani-Aifa, M., Venselaar, H., Kawar, M.N., Tlili, A., van der Zwaag, B., Khan, S.Y., Ayadi, L.,
926 Riazuddin, S.A., Morell, R.J., Griffith, A.J., Charfedine, I., Çaylan, R., Oostrik, J., Karaguzel, A.,
927 Ghorbel, A., Riazuddin, S., Friedman, T.B., Ayadi, H., Kremer, H., 2008. Mutations of LRTOMT, a
928 fusion gene with alternative reading frames, cause nonsyndromic deafness in humans. *Nat.*
929 *Genet.* 40, 1335–1340. doi:10.1038/ng.245
- 930 Alagramam, K.N., Zahorsky-Reeves, J., Wright, C.G., Pawlowski, K.S., Erway, L.C., Stubbs, L.,
931 Woychik, R.P., 2000. Neuroepithelial defects of the inner ear in a new allele of the mouse
932 mutation *Ames waltzer*. *Hear. Res.* 148, 181–191. doi:10.1016/S0378-5955(00)00152-0
- 933 Askew, C., Rochat, C., Pan, B., Asai, Y., Ahmed, H., Child, E., Schneider, B.L., Aebischer, P., Holt, J.R.,
934 2015. *Tmc* gene therapy restores auditory function in deaf mice. *Sci. Transl. Med.* 7, 295ra108.
935 doi:10.1126/scitranslmed.aab1996
- 936 Axelrod, J., Tomchick, R., 1958. Enzymatic O-methylation of epinephrine and other catechols. *J. Biol.*
937 *Chem.* 233, 702–5.
- 938 Basu, A., Lagier, S., Vologodskaia, M., Fabella, B.A., Hudspeth, A.J., 2016. Direct mechanical
939 stimulation of tip links in hair cells through DNA tethers. *Elife* 5. doi:10.7554/eLife.16041
- 940 Beurg, M., Fettiplace, R., Nam, J.-H., Ricci, A.J., 2009. Localization of inner hair cell
941 mechanotransducer channels using high-speed calcium imaging. *Nat. Neurosci.* 12, 553–558.
942 doi:10.1038/nn.2295
- 943 Beurg, M., Kim, K.X., Fettiplace, R., 2014. Conductance and block of hair-cell mechanotransducer
944 channels in transmembrane channel-like protein mutants. *J. Gen. Physiol.* 144, 55–69.
945 doi:10.1085/jgp.201411173

946 Beurg, M., Xiong, W., Zhao, B., Müller, U., Fettiplace, R., 2015. Subunit determination of the
947 conductance of hair-cell mechanotransducer channels. *Proc. Natl. Acad. Sci.* 112, 1589–1594.
948 doi:10.1073/pnas.1420906112

949 Clarke, S., 1992. Protein Isoprenylation and Methylation at Carboxyl-Terminal Cysteine Residues.
950 *Annu. Rev. Biochem.* 61, 355–386. doi:10.1146/annurev.bi.61.070192.002035

951 Corey, D.P., Holt, J.R., 2016. Are TMCs the Mechanotransduction Channels of Vertebrate Hair Cells?
952 *J. Neurosci.* 36, 10921–10926. doi:10.1523/JNEUROSCI.1148-16.2016

953 Corey, D.P., Hudspeth, A.J., 1983. Kinetics of the receptor current in bullfrog saccular hair cells. *J.*
954 *Neurosci.* 3, 962–76.

955 Corns, L.F., Johnson, S.L., Kros, C.J., Marcotti, W., 2016. Tmc1 Point Mutation Affects Ca²⁺
956 Sensitivity and Block by Dihydrostreptomycin of the Mechanoelectrical Transducer Current of
957 Mouse Outer Hair Cells. *J. Neurosci.* 36, 336–49. doi:10.1523/JNEUROSCI.2439-15.2016

958 Corns, L.F., Johnson, S.L., Kros, C.J., Marcotti, W., 2014. Calcium entry into stereocilia drives
959 adaptation of the mechanoelectrical transducer current of mammalian cochlear hair cells. *Proc.*
960 *Natl. Acad. Sci. U. S. A.* 111, 14918–23. doi:10.1073/pnas.1409920111

961 DebRoy, S., Kramarenko, I.I., Ghose, S., Oleinik, N. V., Krupenko, S.A., Krupenko, N.I., 2013. A Novel
962 Tumor Suppressor Function of Glycine N-Methyltransferase Is Independent of Its Catalytic
963 Activity but Requires Nuclear Localization. *PLoS One* 8, e70062.
964 doi:10.1371/journal.pone.0070062

965 Dong, K.B., Maksakova, I.A., Mohn, F., Leung, D., Appanah, R., Lee, S., Yang, H.W., Lam, L.L.,
966 Mager, D.L., Schübeler, D., Tachibana, M., Shinkai, Y., Lorincz, M.C., 2008. DNA methylation in
967 ES cells requires the lysine methyltransferase Gga but not its catalytic activity. *EMBO J.* 27,
968 2691–2701. doi:10.1038/emboj.2008.193

969 Du, X., Schwander, M., Moresco, E.M.Y., Viviani, P., Haller, C., Hildebrand, M.S., Pak, K., Tarantino,
970 L., Roberts, A., Richardson, H., Koob, G., Najmabadi, H., Ryan, A.F., Smith, R.J.H., Muller, U.,
971 Beutler, B., 2008. A catechol-O-methyltransferase that is essential for auditory function in mice
972 and humans. *Proc. Natl. Acad. Sci.* 105, 14609–14614. doi:10.1073/pnas.0807219105

973 Edinger, R.S., Yospin, J., Perry, C., Kleyman, T.R., Johnson, J.P., 2006. Regulation of Epithelial Na⁺
974 Channels (ENaC) by Methylation: A NOVEL METHYLTRANSFERASE STIMULATES ENaC
975 ACTIVITY. *J. Biol. Chem.* 281, 9110–9117. doi:10.1074/jbc.M509232200

976 Ehler, A., Benz, J., Schlatter, D., Rudolph, M.G., 2014. Mapping the conformational space accessible
977 to catechol-O-methyltransferase. *Acta Crystallogr. D. Biol. Crystallogr.* 70, 2163–74.
978 doi:10.1107/S1399004714012917

979 Einhorn, Z., Trapani, J.G., Liu, Q., Nicolson, T., 2012. Rabconnectin3 α promotes stable activity of the
980 H⁺ pump on synaptic vesicles in hair cells. *J. Neurosci.* 32, 11144–56.
981 doi:10.1523/JNEUROSCI.1705-12.2012

982 Erickson, T., French, C.R., Waskiewicz, A.J., 2010. Meis1 specifies positional information in the retina
983 and tectum to organize the zebrafish visual system. *Neural Dev.* 5, 22. doi:10.1186/1749-8104-5-
984 22

985 Falke, J.J., Bass, R.B., Butler, S.L., Chervitz, S.A., Danielson, M.A., 1997. The two-component
986 signaling pathway of bacterial chemotaxis: a molecular view of signal transduction by receptors,
987 kinases, and adaptation enzymes. *Annu. Rev. Cell Dev. Biol.* 13, 457–512.
988 doi:10.1146/annurev.cellbio.13.1.457

989 Gale, J.E., Meyers, J.R., Corwin, J.T., 2000. Solitary hair cells are distributed throughout the
990 extramacular epithelium in the bullfrog's sacculle. *J. Assoc. Res. Otolaryngol.* 1, 172–82.

991 Kalay, E., Caylan, R., Kiroglu, A.F., Yasar, T., Collin, R.W.J., Heister, J.G.A.M., Oostrik, J., Cremers,

992 C.W.R.J., Brunner, H.G., Karaguzel, A., Kremer, H., 2007. A novel locus for autosomal recessive
993 nonsyndromic hearing impairment, DFNB63, maps to chromosome 11q13.2-q13.4. *J. Mol. Med.*
994 (Berl). 85, 397–404. doi:10.1007/s00109-006-0136-3

995 Kawashima, Y., Géléoc, G.S.G., Kurima, K., Labay, V., Lelli, A., Asai, Y., Makishima, T., Wu, D.K.,
996 Della Santina, C.C., Holt, J.R., Griffith, A.J., 2011. Mechanotransduction in mouse inner ear hair
997 cells requires transmembrane channel-like genes. *J. Clin. Invest.* 121, 4796–4809.
998 doi:10.1172/JCI60405

999 Kazmierczak, P., Sakaguchi, H., Tokita, J., Wilson-Kubalek, E.M., Milligan, R.A., Müller, U., Kachar,
1000 B., 2007. Cadherin 23 and protocadherin 15 interact to form tip-link filaments in sensory hair
1001 cells. *Nature* 449, 87–91. doi:10.1038/nature06091

1002 Kettleborough, R.N.W., Busch-Nentwich, E.M., Harvey, S.A., Dooley, C.M., de Bruijn, E., van Eeden,
1003 F., Sealy, I., White, R.J., Herd, C., Nijman, I.J., Fényes, F., Mehroke, S., Scahill, C., Gibbons, R.,
1004 Wali, N., Carruthers, S., Hall, A., Yen, J., Cuppen, E., Stemple, D.L., 2013. A systematic genome-
1005 wide analysis of zebrafish protein-coding gene function. *Nature* 496, 494–7.
1006 doi:10.1038/nature11992

1007 Khan, S.Y., Riazuddin, S., Tariq, M., Anwar, S., Shabbir, M.I., Riazuddin, S.A., Khan, S.N., Husnain, T.,
1008 Ahmed, Z.M., Friedman, T.B., Riazuddin, S., 2007. Autosomal recessive nonsyndromic deafness
1009 locus DFNB63 at chromosome 11q13.2–q13.3. *Hum. Genet.* 120, 789–793. doi:10.1007/s00439-
1010 006-0275-1

1011 Kindt, K.S., Finch, G., Nicolson, T., 2012. Kinocilia Mediate Mechanosensitivity in Developing
1012 Zebrafish Hair Cells. *Dev. Cell* 23, 329–341. doi:10.1016/j.devcel.2012.05.022

1013 Kros, C.J., Rusch, A., Richardson, G.P., 1992. Mechano-Electrical Transducer Currents in Hair Cells of
1014 the Cultured Neonatal Mouse Cochlea. *Proc. R. Soc. London B Biol. Sci.* 249.

1015 Kurima, K., Ebrahim, S., Pan, B., Sedlacek, M., Sengupta, P., Millis, B.A., Cui, R., Nakanishi, H.,
1016 Fujikawa, T., Kawashima, Y., Choi, B.Y., Monahan, K., Holt, J.R., Griffith, A.J., Kachar, B., 2015.
1017 TMC1 and TMC2 Localize at the Site of Mechanotransduction in Mammalian Inner Ear Hair Cell
1018 Stereocilia. *Cell Rep.* 12, 1606–1617. doi:10.1016/j.celrep.2015.07.058

1019 Kurima, K., Peters, L.M., Yang, Y., Riazuddin, S., Ahmed, Z.M., Naz, S., Arnaud, D., Drury, S., Mo, J.,
1020 Makishima, T., Ghosh, M., Menon, P.S.N., Deshmukh, D., Oddoux, C., Ostrer, H., Khan, S.,
1021 Riazuddin, S., Deininger, P.L., Hampton, L.L., Sullivan, S.L., Battey, J.F., Keats, B.J.B., Wilcox,
1022 E.R., Friedman, T.B., Griffith, A.J., 2002. Dominant and recessive deafness caused by mutations
1023 of a novel gene, TMC1, required for cochlear hair-cell function. *Nat. Genet.* 30, 277–284.
1024 doi:10.1038/ng842

1025 Kwan, K.M., Fujimoto, E., Grabher, C., Mangum, B.D., Hardy, M.E., Campbell, D.S., Parant, J.M.,
1026 Yost, H.J., Kanki, J.P., Chien, C.-B., 2007. The Tol2kit: a multisite gateway-based construction
1027 kit for Tol2 transposon transgenesis constructs. *Dev. Dyn.* 236, 3088–99.
1028 doi:10.1002/dvdy.21343

1029 Law, B.J.C., Bennett, M.R., Thompson, M.L., Levy, C., Shepherd, S.A., Leys, D., Micklefield, J., 2016.
1030 Effects of Active-Site Modification and Quaternary Structure on the Regioselectivity of
1031 Catechol- O -Methyltransferase. *Angew. Chemie Int. Ed.* 55, 2683–2687.
1032 doi:10.1002/anie.201508287

1033 Longo-Guess, C.M., Gagnon, L.H., Cook, S.A., Wu, J., Zheng, Q.Y., Johnson, K.R., 2005. A missense
1034 mutation in the previously undescribed gene Tmhs underlies deafness in hurry-scurry (hscy)
1035 mice. *Proc. Natl. Acad. Sci.* 102, 7894–7899. doi:10.1073/pnas.0500760102

1036 Maeda, R., Kindt, K.S., Mo, W., Morgan, C.P., Erickson, T., Zhao, H., Clemens-Grisham, R., Barr-
1037 Gillespie, P.G., Nicolson, T., 2014. Tip-link protein protocadherin 15 interacts with

1038 transmembrane channel-like proteins TMC1 and TMC2. *Proc. Natl. Acad. Sci.* 111, 12907–12912.
1039 doi:10.1073/pnas.1402152111

1040 Maeda, R., Pacentine, I. V., Erickson, T., Nicolson, T., 2017. Functional Analysis of the
1041 Transmembrane and Cytoplasmic Domains of Pcdh15a in Zebrafish Hair Cells. *J. Neurosci.* 37,
1042 3231–3245. doi:10.1523/JNEUROSCI.2216-16.2017

1043 Meeker, N.D., Hutchinson, S.A., Ho, L., Trede, N.S., 2007. Method for isolation of PCR-ready
1044 genomic DNA from zebrafish tissues. *Biotechniques* 43, 610, 612, 614.

1045 Meyers, J.R., MacDonald, R.B., Duggan, A., Lenzi, D., Standaert, D.G., Corwin, J.T., Corey, D.P.,
1046 2003. Lighting up the senses: FM1-43 loading of sensory cells through nonselective ion channels.
1047 *J. Neurosci.* 23, 4054–65.

1048 Mitchem, K.L., Hibbard, E., Beyer, L.A., Bosom, K., Dootz, G.A., Dolan, D.F., Johnson, K.R., Raphael,
1049 Y., Kohrman, D.C., 2002. Mutation of the novel gene *Tmie* results in sensory cell defects in the
1050 inner ear of spinner, a mouse model of human hearing loss DFNB6. *Hum. Mol. Genet.* 11, 1887–
1051 98.

1052 Nicolson, T., Rüsçh, A., Friedrich, R.W., Granato, M., Ruppertsberg, J.P., Nüsslein-Volhard, C., 1998.
1053 Genetic analysis of vertebrate sensory hair cell mechanosensation: the zebrafish circler mutants.
1054 *Neuron* 20, 271–83. doi:10.1016/S0896-6273(00)80455-9

1055 Nishikawa, S., Sasaki, F., 1996. Internalization of styryl dye FM1-43 in the hair cells of lateral line
1056 organs in *Xenopus* larvae. *J. Histochem. Cytochem.* 44, 733–741. doi:10.1177/44.7.8675994

1057 Olt, J., Johnson, S.L., Marcotti, W., 2014. In vivo and in vitro biophysical properties of hair cells from
1058 the lateral line and inner ear of developing and adult zebrafish. *J. Physiol.* 592, 2041–2058.
1059 doi:10.1113/jphysiol.2013.265108

1060 Olt, J., Ordoobadi, A.J., Marcotti, W., Trapani, J.G., 2016. Physiological recordings from the zebrafish

1061 lateral line, in: *Methods in Cell Biology*. pp. 253–279. doi:10.1016/bs.mcb.2016.02.004

1062 Pan, B., Géléoc, G.S., Asai, Y., Horwitz, G.C., Kurima, K., Ishikawa, K., Kawashima, Y., Griffith, A.J.,
1063 Holt, J.R., 2013. TMC1 and TMC2 Are Components of the Mechanotransduction Channel in Hair
1064 Cells of the Mammalian Inner Ear. *Neuron* 79, 504–515. doi:10.1016/j.neuron.2013.06.019

1065 Perreault, A., Gascon, S., D'Amours, A., Aletta, J.M., Bachand, F., 2009. A Methyltransferase-
1066 independent Function for Rmt3 in Ribosomal Subunit Homeostasis. *J. Biol. Chem.* 284, 15026–
1067 15037. doi:10.1074/jbc.M109.004812

1068 Pickles, J.O., Comis, S.D., Osborne, M.P., 1984. Cross-links between stereocilia in the guinea pig
1069 organ of Corti, and their possible relation to sensory transduction. *Hear. Res.* 15, 103–112.
1070 doi:10.1016/0378-5955(84)90041-8

1071 Rutherford, K., Le Trong, I., Stenkamp, R.E., Parson, W.W., 2008. Crystal Structures of Human 108V
1072 and 108M Catechol O-Methyltransferase. *J. Mol. Biol.* 380, 120–130.
1073 doi:10.1016/j.jmb.2008.04.040

1074 Scheffer, D.I., Shen, J., Corey, D.P., Chen, Z.-Y., 2015. Gene Expression by Mouse Inner Ear Hair Cells
1075 during Development. *J. Neurosci.* 35, 6366–6380. doi:10.1523/JNEUROSCI.5126-14.2015

1076 Seiler, C., Ben-David, O., Sidi, S., Hendrich, O., Rusch, A., Burnside, B., Avraham, K.B., Nicolson, T.,
1077 2004. Myosin VI is required for structural integrity of the apical surface of sensory hair cells in
1078 zebrafish. *Dev. Biol.* 272, 328–38. doi:10.1016/j.ydbio.2004.05.004

1079 Seiler, C., Finger-Baier, K.C., Rinner, O., Makhankov, Y. V, Schwarz, H., Neuhauss, S.C.F., Nicolson,
1080 T., 2005. Duplicated genes with split functions: independent roles of protocadherin15
1081 orthologues in zebrafish hearing and vision. *Development* 132, 615–23. doi:10.1242/dev.01591

1082 Seiler, C., Nicolson, T., 1999. Defective calmodulin-dependent rapid apical endocytosis in zebrafish
1083 sensory hair cell mutants. *J. Neurobiol.* 41, 424–34.

1084 Shen, J., Scheffer, D.I., Kwan, K.Y., Corey, D.P., 2015. SHIELD: an integrative gene expression
1085 database for inner ear research. Database (Oxford). 2015, bavo71. doi:10.1093/database/bavo71

1086 Shin, J.-B., Krey, J.F., Hassan, A., Metlagel, Z., Tauscher, A.N., Pagana, J.M., Sherman, N.E., Jeffery,
1087 E.D., Spinelli, K.J., Zhao, H., Wilmarth, P.A., Choi, D., David, L.L., Auer, M., Barr-Gillespie, P.G.,
1088 2013. Molecular architecture of the chick vestibular hair bundle. Nat. Neurosci. 16, 365–74.
1089 doi:10.1038/nn.3312

1090 Sipe, C.W., Liu, L., Lee, J., Grimsley-Myers, C., Lu, X., 2013. Lis1 mediates planar polarity of auditory
1091 hair cells through regulation of microtubule organization. Development 140, 1785–95.
1092 doi:10.1242/dev.089763

1093 Steel, K.P., Bock, G.R., 1980. The nature of inherited deafness in deafness mice. Nature 288, 159–61.

1094 Thisse, C., Thisse, B., 2008. High-resolution in situ hybridization to whole-mount zebrafish embryos.
1095 Nat. Protoc. 3, 59–69. doi:10.1038/nprot.2007.514

1096 Tlili, A., Masmoudi, S., Dhouib, H., Bouaziz, S., Rebeh, I. Ben, Chouchen, J., Turki, K., Benzina, Z.,
1097 Charfedine, I., Drira, M., Ayadi, H., 2007. Localization of a novel autosomal recessive non-
1098 syndromic hearing impairment locus DFNB63 to chromosome 11q13.3-q13.4. Ann. Hum. Genet.
1099 71, 271–5. doi:10.1111/j.1469-1809.2006.00337.x

1100 Tu, L., Banfield, D.K., 2010. Localization of Golgi-resident glycosyltransferases. Cell. Mol. Life Sci. 67,
1101 29–41. doi:10.1007/s00018-009-0126-z

1102 UniProt Consortium, 2015. UniProt: a hub for protein information. Nucleic Acids Res. 43, D204-12.
1103 doi:10.1093/nar/gku989

1104 Vidgren, J., Svensson, L.A., Liljas, A., 1994. Crystal structure of catechol O-methyltransferase. Nature
1105 368, 354–358. doi:10.1038/368354a0

1106 Wu, Z., Muller, U., 2016. Molecular Identity of the Mechanotransduction Channel in Hair Cells: Not

1107 Quiet There Yet. *J. Neurosci.* 36, 10927–10934. doi:10.1523/JNEUROSCI.1149-16.2016

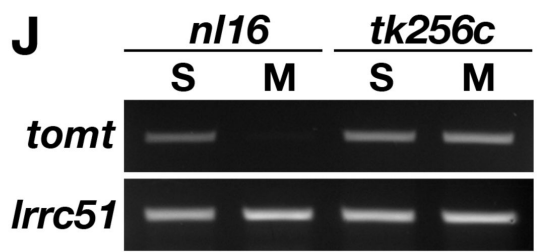
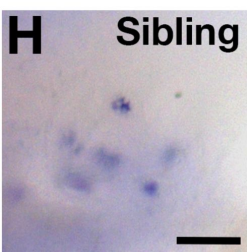
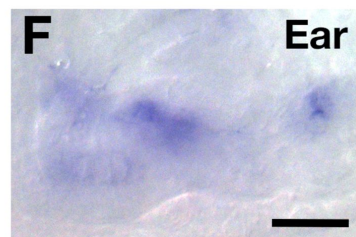
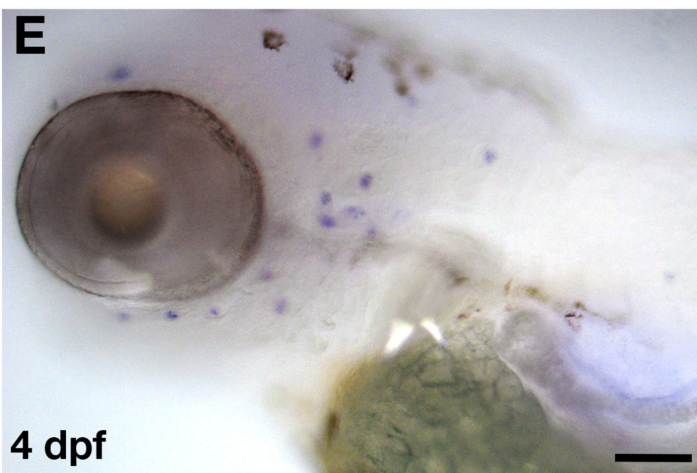
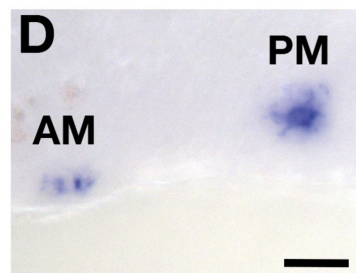
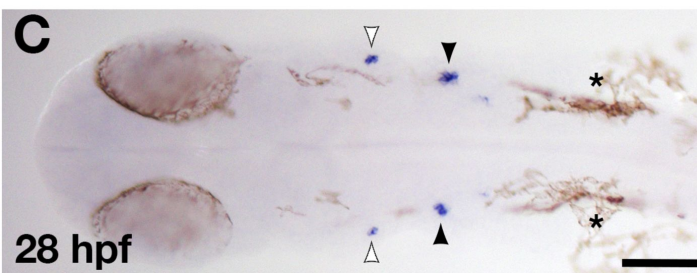
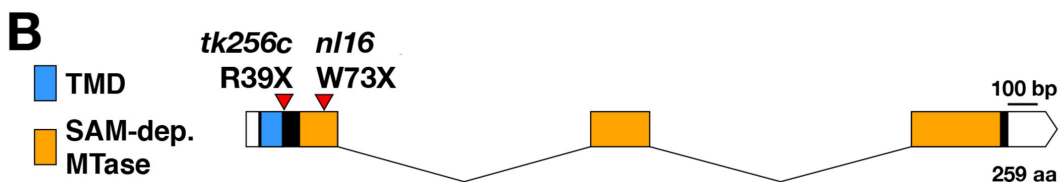
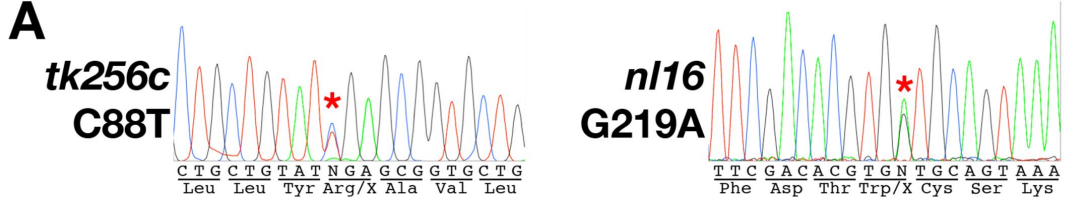
1108 Xiong, W., Grillet, N., Elledge, H.M., Wagner, T.F.J., Zhao, B., Johnson, K.R., Kazmierczak, P., Müller,
1109 U., 2012. TMHS Is an Integral Component of the Mechanotransduction Machinery of Cochlear
1110 Hair Cells. *Cell* 151, 1283–1295. doi:10.1016/j.cell.2012.10.041

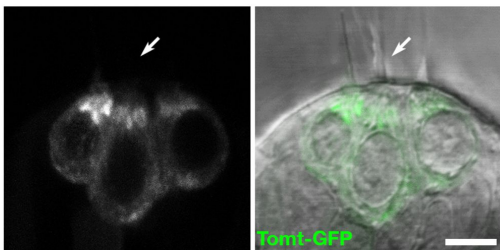
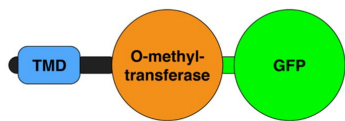
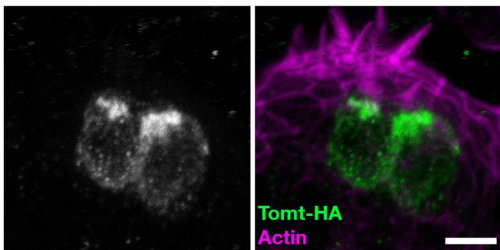
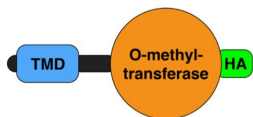
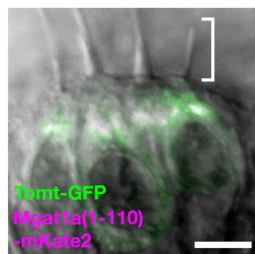
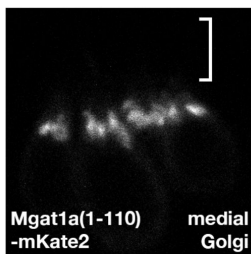
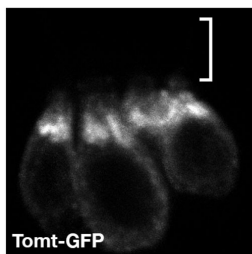
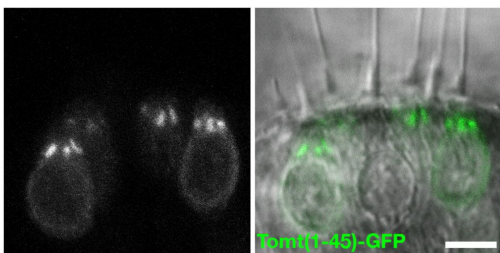
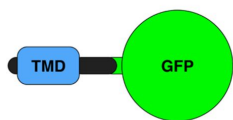
1111 Zhang, J., Klinman, J.P., 2011. Enzymatic methyl transfer: Role of an active site residue in generating
1112 active site compaction that correlates with catalytic efficiency. *J. Am. Chem. Soc.* 133, 17134–
1113 17137. doi:10.1021/ja207467d

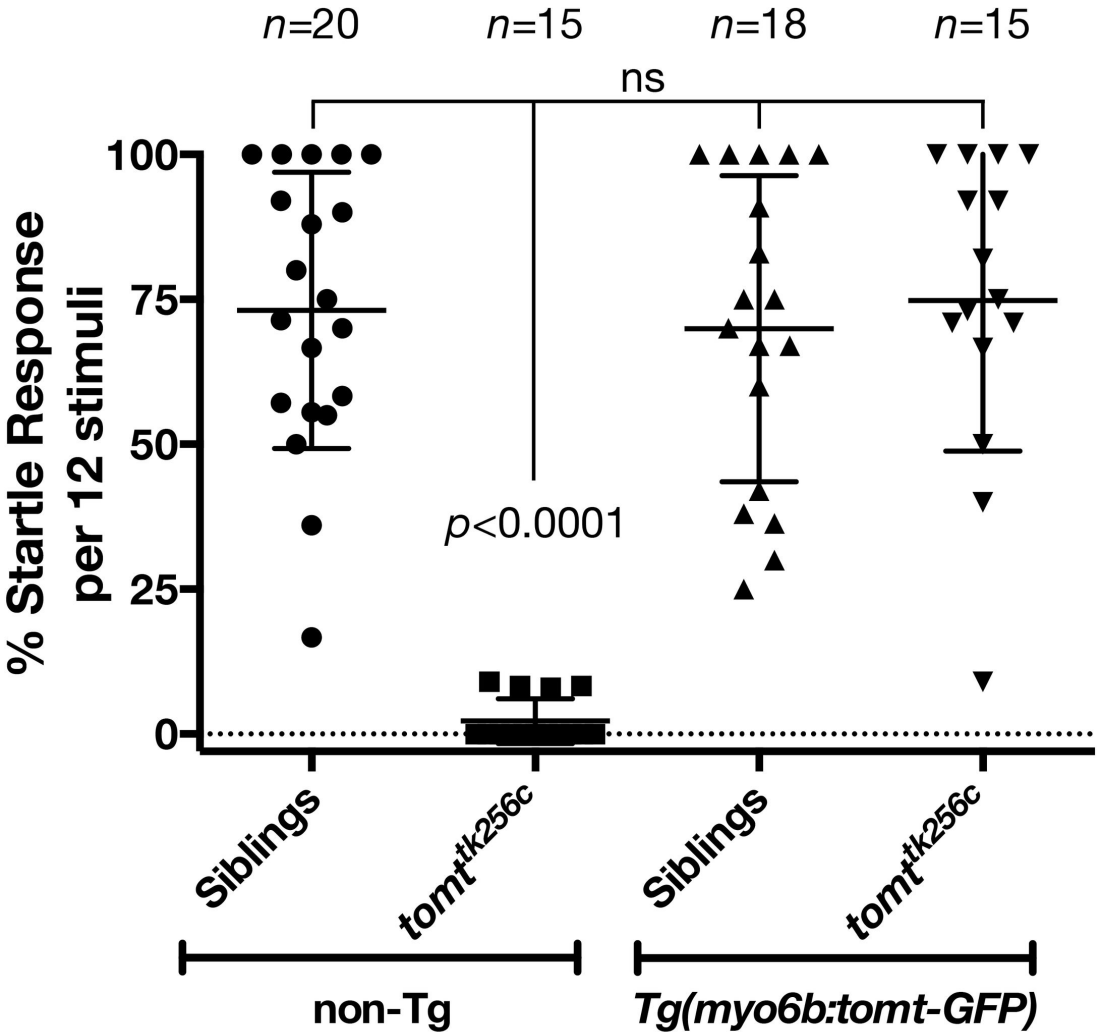
1114 Zhang, J., Kulik, H.J., Martinez, T.J., Klinman, J.P., 2015. Mediation of donor-acceptor distance in an
1115 enzymatic methyl transfer reaction. *Proc. Natl. Acad. Sci. U. S. A.* 112, 7954–9.
1116 doi:10.1073/pnas.1506792112

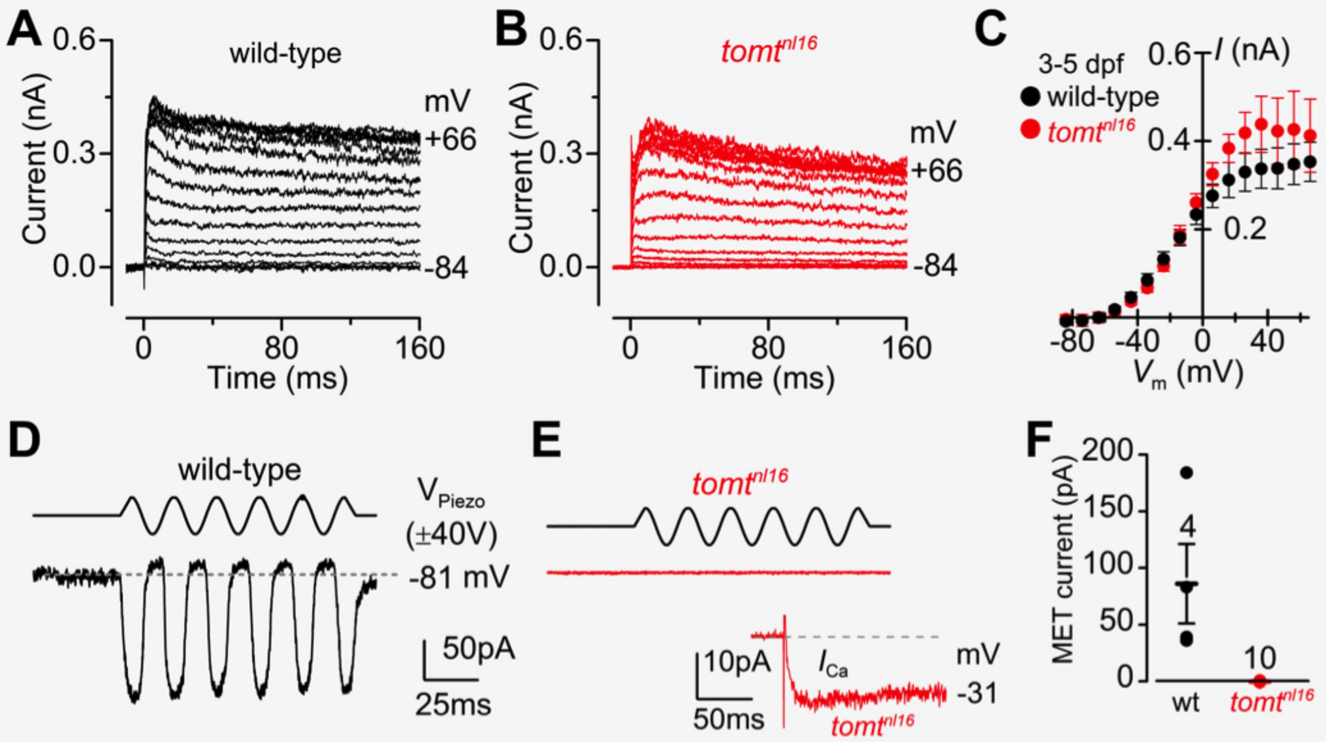
1117 Zhao, B., Wu, Z., Grillet, N., Yan, L., Xiong, W., Harkins-Perry, S., Müller, U., 2014. TMIE Is an
1118 Essential Component of the Mechanotransduction Machinery of Cochlear Hair Cells. *Neuron* 84,
1119 954–967. doi:10.1016/j.neuron.2014.10.041

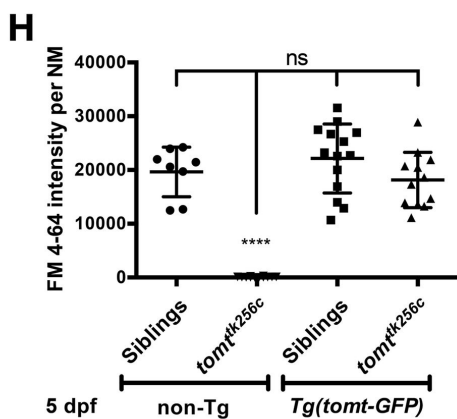
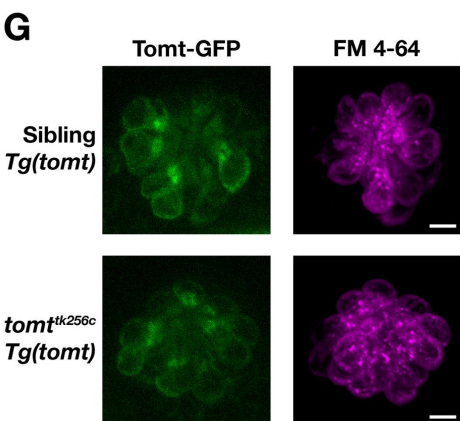
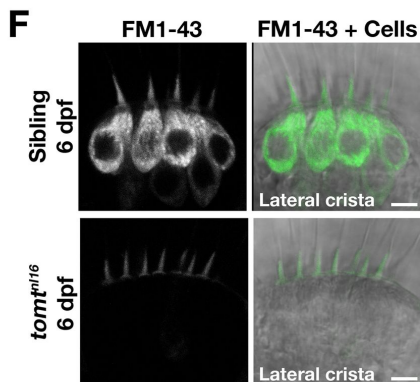
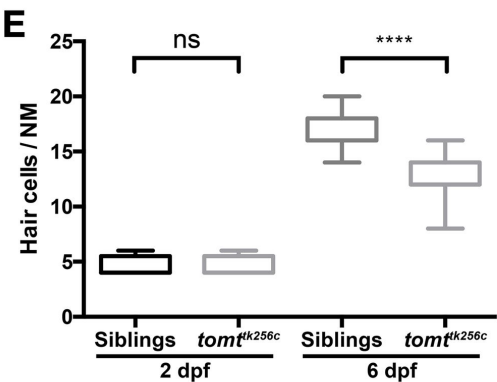
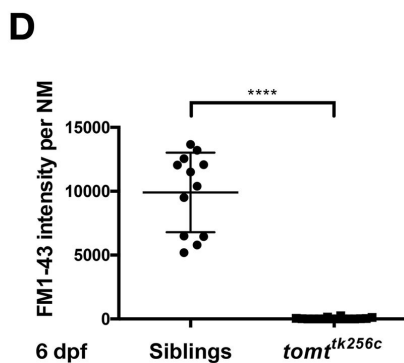
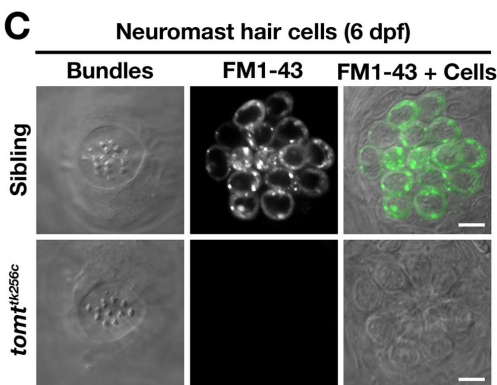
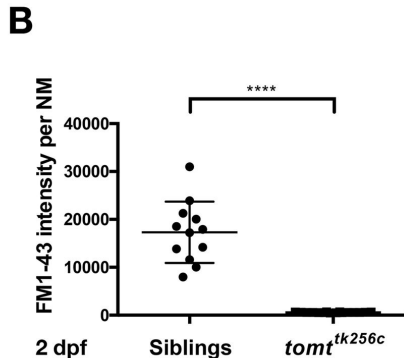
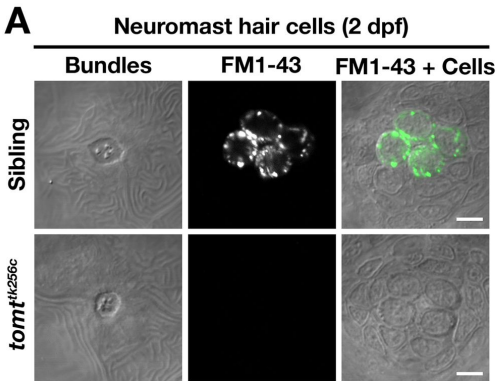
1120

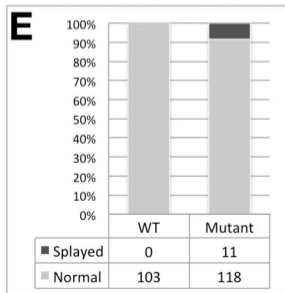
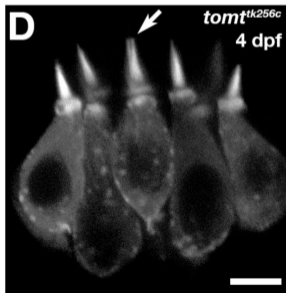
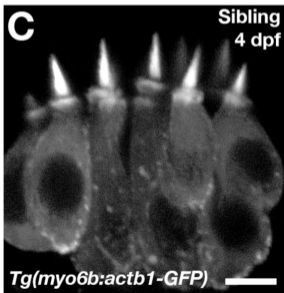
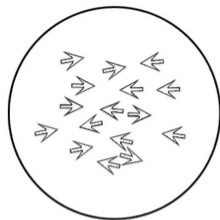
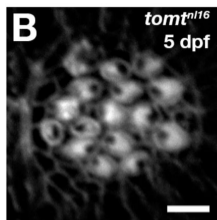
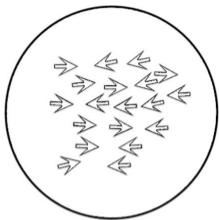
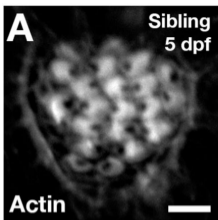


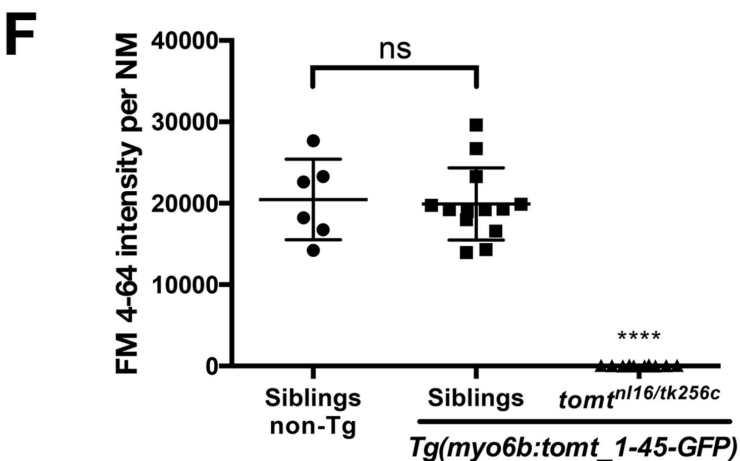
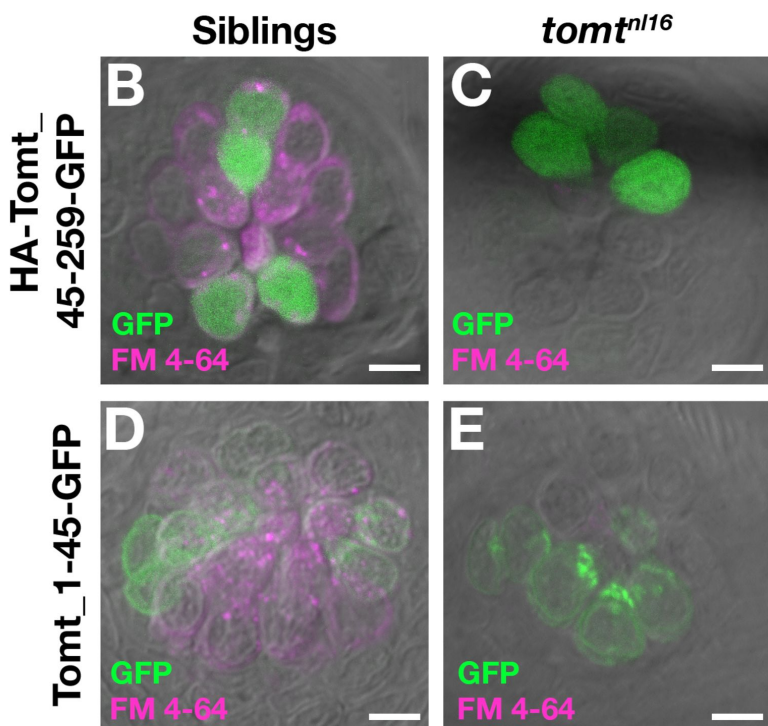
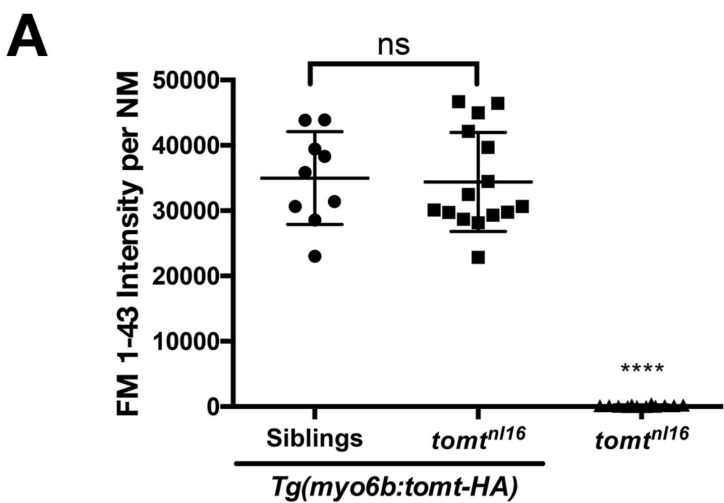
A**B****C****D**

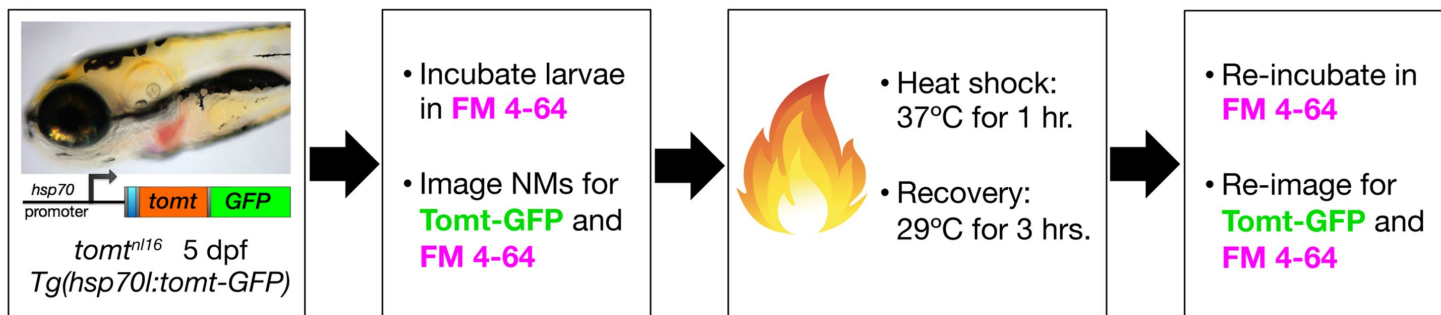
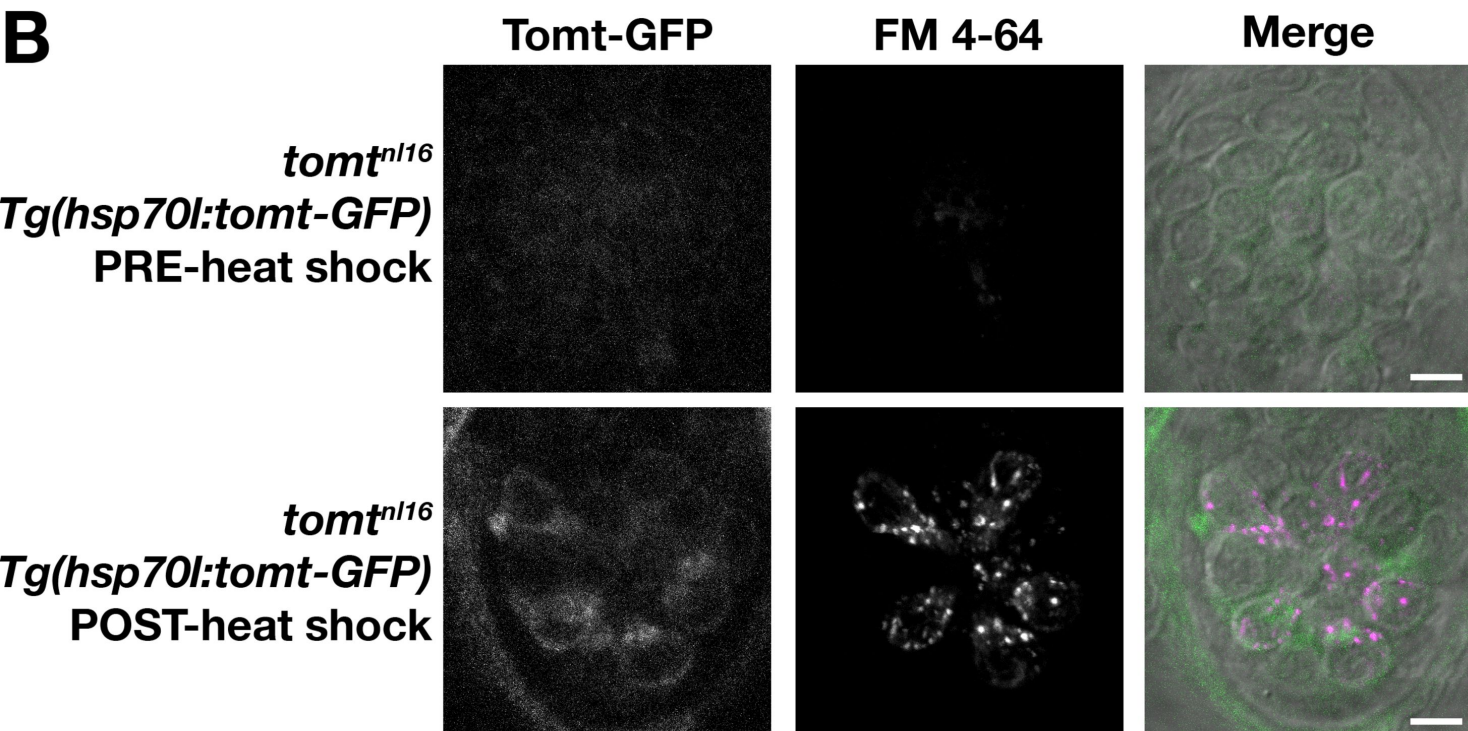
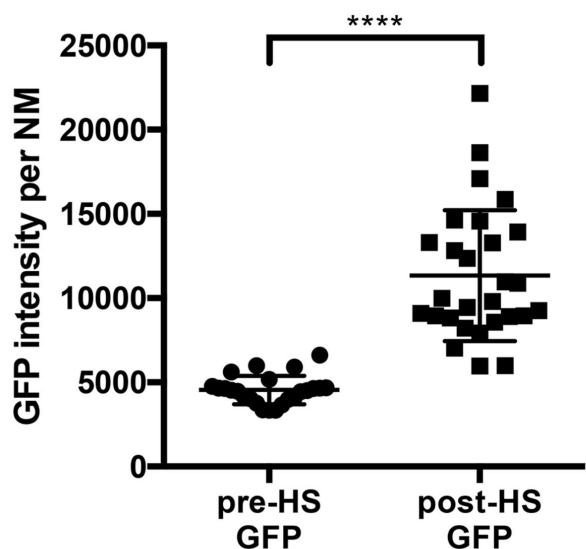
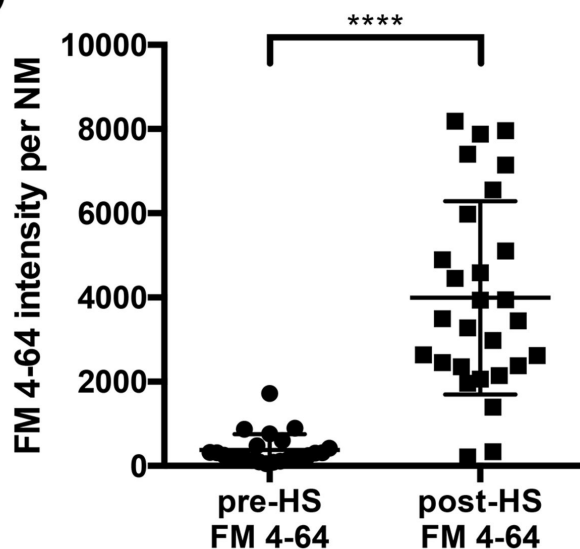








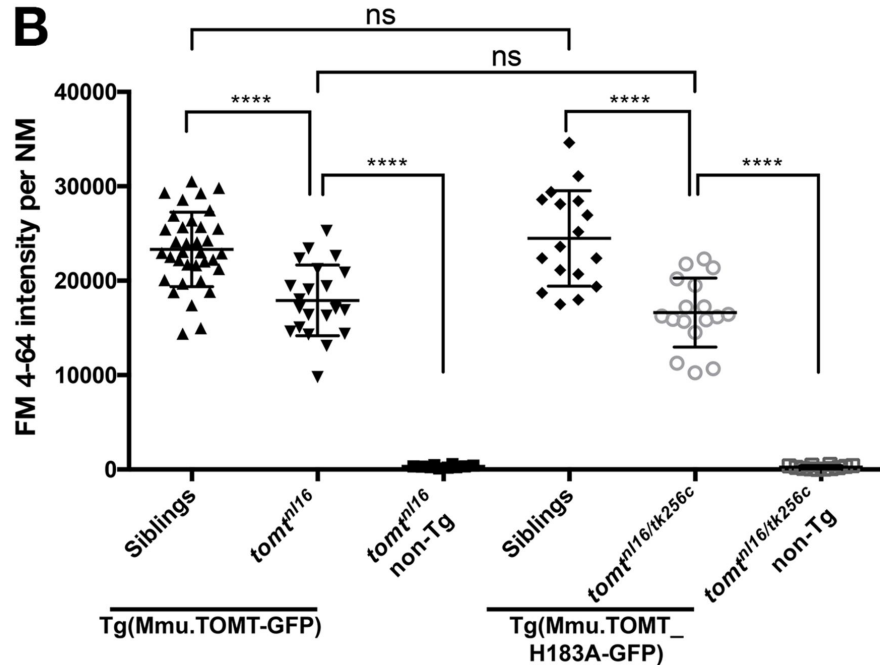
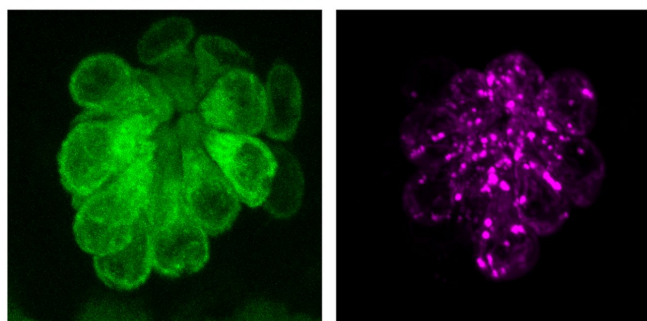
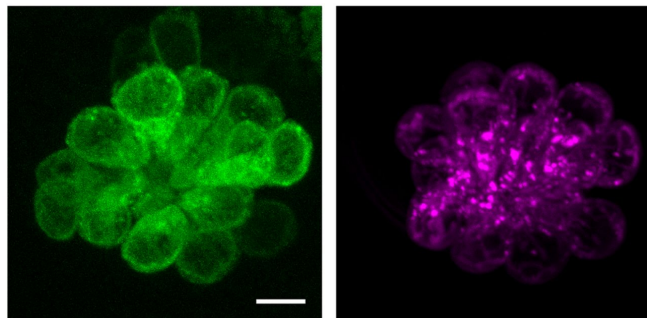


A**B****C****D**

A

Pink: Mg²⁺ binding
Blue: SAM binding
Yellow: Substrate binding

Danio Comta	DFVFLDHWKDRYVPD
Human COMT	DMVFLDHWKDRYLPD
Danio Tomt	DLVLMDHWKRCYLPD
Coelacanth Tomt	DFVFM ^Y DHWKRCYLKD
Xenopus Tomt	DFIFMD ^Y HGKRCYLKD
Chicken LRTOMT	DFVFM ^Y DHWKRCYLKD
Opossum TOMT	GLVLLGHRPRCYLRD
Mouse TOMT	DLVLLAHRPRYYLRD
Human LRTOMT	DLVLLAHRPRCYLRD
 * * : *

B**C****Mmu.TOMT-GFP****FM 4-64****D****Mmu.TOMT_H183A-GFP****FM 4-64**